

What is the best RNN-cell structure for forecasting each time series behavior?

Rohaifa Khaldi^{a,*}, Abdellatif El Afia^b, Raddouane Chiheb^b, Siham Tabik^a

^a*Dept. of Computer Science and Artificial Intelligence, Andalusian Research Institute in Data Science and Computational Intelligence, DaSCI, University of Granada, 18071, Granada, Spain*

^b*ENSIAS, Mohammed V University of Rabat, 10170, Rabat, Morocco*

Abstract

It is unquestionable that time series forecasting is of paramount importance in many fields. The most used machine learning models to address time series forecasting tasks are Recurrent Neural Networks (RNNs). Typically, those models are built using one of the three most popular cells, ELMAN, Long-Short Term Memory (LSTM), or Gated Recurrent Unit (GRU) cells, each cell has a different structure and implies a different computational cost. However, it is not clear why and when to use each RNN-cell structure. Actually, there is no comprehensive characterization of all the possible time series behaviors and no guidance on what RNN cell structure is the most suitable for each behavior. The objective of this study is two-fold: it presents a comprehensive taxonomy of all-time series behaviors (deterministic, random-walk, nonlinear, long-memory, and chaotic), and provides insights into the best RNN cell structure for each time series behavior. We conducted two experiments: (1) The first experiment evaluates and analyzes the role of each component in the LSTM-Vanilla cell by creating 11 variants based on one alteration in its basic architecture (removing, adding, or substituting one cell component). (2) The second experiment evaluates and analyzes the performance of 20 possible RNN-cell structures. Our results showed that the MGU-SLIM3 cell is the most recommended for deterministic and nonlinear behaviors, the MGU-SLIM2 cell is the most suitable for random-walk behavior, FB1 cell is advocated for long-memory behavior, and LSTM-SLIM1 for chaotic behavior.

Keywords: Forecasting; Time series; Times series behavior; RNN models; LSTM cells

1. Introduction

Many real-world prediction problems involve a temporal dimension and typically require the estimation of numerical sequential data referred to as time series forecasting. Time series forecasting is one of the major stones in data science playing a pivotal role in almost all domains, including meteorology (Murat et al. 2018), natural disasters control (Erdelj et al. 2017), energy (Bourdeau et al. 2019), manufacturing (Wang and Chen 2018), finance (Liu 2019), econometrics (Siami-Namini and Namin 2018), telecommunication (Maeng et al.

*Corresponding author.

Email addresses: rohaifa@ugr.es (Rohaifa Khaldi), abdellatif.elafia@ensias.um5.ac.ma (Abdellatif El Afia), raddouane.chiheb@ensias.um5.ac.ma (Raddouane Chiheb), siham@ugr.es (Siham Tabik)

2020), healthcare (Khaldi et al. 2019b) to name a few. Accurate time series forecasting requires robust forecasting models.

Currently, Recurrent Neural Network (RNN) models are one of the most popular machine learning models in sequential data modeling, including natural language, image/video captioning, and forecasting (Sutskever et al. 2014, Vinyals et al. 2015, Chimmula and Zhang 2020). Such RNN models are built as a sequence of the same cell structure, for example, ELMAN cell, Long-Short Term Memory (LSTM) cell or Gated Recurrent Unit (GRU) cell. The simplest RNN cell is ELMAN, it includes one layer of hidden neurons. While, LSTM and GRU cells incorporate a gating mechanism, three gates in LSTM and two gates in GRU, where each gate is a layer of hidden neurons. Many other cell structures have been introduced in the literature (Zhou et al. 2016, Lu and Salem 2017, Mikolov et al. 2014, Pulver and Lyu 2017). However, to solve time series forecasting tasks, the building of RNN models is typically limited to the three aforementioned cell structures (Sezer et al. 2020, Runge and Zmeureanu 2021, Liu et al. 2021, Rajagukguk et al. 2020, Alkhayat and Mehmood 2021), as they provide very good accuracy (Runge and Zmeureanu 2021, Sezer et al. 2020).

Nevertheless, building robust RNN models for time series forecasting is still a challenging task as there does not exist yet a clear understanding of times series data itself and hence there exist very little knowledge about what cell structure is the most appropriate for each data type. In general, when facing a new problem, practitioners select one of the most popular cells, usually LSTM, and use it as a building block for the RNN model without any guarantee on the appropriateness of this cell to the current data. The objective of this work is two-fold. It presents a comprehensive characterization of time series behaviors, and provides guidelines on the best RNN cell structure for each behavior. As far as we know, this is the first work in providing such insights. The main contributions of this study can be summarized as follows:

- Provide a better understanding of times series data by presenting a comprehensive characterization of their behaviors.
- Determine the most appropriate cell structure for each time series behavior (i.e., whether a specific cell structure should be avoided for certain behaviors).
- Identify differences in predictability between behaviors (i.e., whether certain behaviors are easier or harder to predict across all cell models).
- Provide useful guidelines that can assist decision-makers and scholars in the process of selecting the most suitable RNN-cell structure from both, a computational and performance point of views.

The remainder of this study is organized as follows: Section 2 states the related works. Section 3 presents a taxonomy of time series behaviors. Section 4 presents a taxonomy of RNN cells. Section 5 describes the experiment. Section 6 exhibits and discuss the obtained results. Finally, the last section concludes the findings and spots light on future research directions.

2. Related works

The last decades have known an explosion of time series data acquired by automated data collection devices such as monitors, IoT devices, and sensors (Murat et al. 2018, Erdelj et al. 2017, Bourdeau et al. 2019). The collected time series describe different quantitative values: stock price, amount of sales, electricity load demand, weather temperature, etc. In parallel, a large number of comparative studies have been carried out in the forecasting area (Parmezan et al. 2019, Godahewa et al. 2021, Athiyarath et al. 2020, Divina et al. 2019, Choubin et al. 2018, Sagheer and Kotb 2019, Bianchi et al. 2017). These studies can be divided into two categories: (1) the first category tries to find a universal forecasting model (Parmezan et al. 2019, Godahewa et al. 2021, Athiyarath et al. 2020). They compare multiple models on a set of datasets from different fields to conclude which model is the universal predictor. The selection of the used datasets is not based on any clear criteria. Whereas, (2) the second category focuses on selecting the most performing forecasting model (Divina et al. 2019, Choubin et al. 2018, Sagheer and Kotb 2019, Bianchi et al. 2017). They compare a set of models on one or multiple datasets coming from a the same field. Nevertheless, the best predictor does not ensure stable performance over different datasets even if they come from the same field. Actually, after an extensive analysis on highly diverse datasets, Keogh and Kasetty (2003) demonstrated that there is a need for more comprehensive time series benchmarks and more careful evaluations in the data mining community. In addition, datasets should have a large size to train and test the models, and incorporate specific behaviors that challenge their modeling. Such knowledge of the dataset properties is required to facilitate a better interpretation of the modeling results.

The natural approach to create such benchmarking time series datasets is to collect data from real applications. For instance, the NN5 dataset (Crone 2008), the CIF 2016 dataset (Godahewa et al. 2020), the M4 dataset (Makridakis et al. 2018), and the Monash archive that gather 20 publicly available time series datasets (Godahewa et al. 2021). Although, real time series are always business-oriented which make them either proprietary or expensive to obtain (Dau et al. 2019), they can take decades to become mature and ready to be used for machine learning purposes, their diversity testing is tedious (Dau et al. 2019, Spiliotis et al. 2020), and most importantly, their Data Generation Processes (DGPs) are unknown which make the interpretation of the models and the explanation of their decisions challenging.

An alternative solution is to generate synthetic time series datasets with known embedded patterns (Olson et al. 2017). For instance, Zhang and Qi (2005) investigated the issue of how to effectively model artificial time series with deterministic behavior due to the existence of trend and seasonality using Artificial Neural Networks (ANNs). López-Caraballo et al. (2016) examined ANNs on time series with noiseless and noisy chaotic behavior generated by Mackey-Glass series. Li and Lin (2016) applied the Self-Constructing Fuzzy Neural Network (SCFNN) on chaotic time series including Logistic and Henon data. Yeo (2017) evaluated the performance of LSTM on three different time series with chaotic behavior (delay-time chaotic dynamical systems, Mackey-Glass and Ikeda equations). Fischer et al. (2018) presented an experimental evaluation of seven machine learning models applied on a set of eight DGPs reflecting linear and nonlinear

behaviors. Parmezan et al. (2019) used 40 synthetic datasets of deterministic, stochastic and chaotic time series to compare eleven parametric and non-parametric models. Kang et al. (2020) used mixture autoregressive (MAR) models to create GRATIS dataset based on which they compared different statistical models. However, all the aforementioned studies remain non comprehensive of the main time series behaviors that can be faced in real datasets.

Another categorization of these comparative studies can be made based on the types of the evaluated models. Here, three categories can be set: (1) Studies based on parametric models where scientists try to evaluate the forecasting performance of different statistical models (Godaheva et al. 2021, Yu et al. 2020, Kim and Jung 2018). (2) Studies based on non-parametric models where they assess the performance of machine learning models (Granata 2019, Dudek 2016, Sagheer and Kotb 2019). (3) Studies based on parametric and non-parametric models where both types of models are compared (Parmezan et al. 2019, Khaldi et al. 2019a, Yamak et al. 2019, Siami-Namini and Namin 2018). RNNs are one of the most used machine learning models in time series forecasting (Sezer et al. 2020). Nevertheless, their usage is limited to three RNN variants (ELMAN, LSTM, and GRU). In the financial field, Sezer et al. (2020) reported that from 2005 to 2019, 52.5% of publications used RNN models to perform time series forecasting, where LSTM model represents 60.4%, ELMAN (vanilla RNN) represents 29.7%, and GRU represents 9.89%. In the energy field, Runge and Zmeureanu (2021) stated in their review that ELMAN, GRU, and LSTM are the main applied deep learning models to building energy forecasting. In the environmental field, Liu et al. (2021) asserted in their review, from 2015 to 2020, that LSTM and GRU are the most practical RNN models in the air quality forecasting. In the renewable energy field, Rajagukguk et al. (2020) reviewed, from 2005 to 2020, that in the photovoltaic power forecasting, 60% of publications used LSTM, 20% used ELMAN, and 13% used GRU. While, in the solar irradiance forecasting, they reported that LSTM represent 44% of the used deep learning models, ELMAN represents 25%, and GRU 19%. Similarly, Alkhayat and Mehmood (2021) reported in their review, from 2016 to 2020, that ELMAN, LSTM, and GRU are the only RNN models used in wind and solar energy forecasting. They outlined that the usage of RNNs within this field increased from 2% in 2016 to 25% in 2020.

Therefore, there is a strong need for a comprehensive analysis of different types of RNN models, including the above three variants, in forecasting the main time series behaviors, and a strong need for an RNN-based models guide to assist practitioners in their process of selection and structure of the best RNN cell for each time series behavior.

3. Taxonomy of times series behaviors

As far as we know, this is the first work in introducing a complete formal characterization of real-world time series. Time series emerging from real-world applications can either follow a stochastic mechanism or a chaotic mechanism, and are usually contaminated by white noise (Wales 1991, Cencini et al. 2000, Zunino et al. 2012, Box et al. 2015, Boaretto et al. 2021).

3.1. Stochastic behavior

In the stochastic behavior, real times series are generated by a random stable system, and can exhibit the following behaviors:

1. Deterministic behavior. These time series are characterized by the existence of deterministic patterns. They usually incorporate at least one of the following patterns: increasing or decreasing deterministic trend, simple deterministic seasonality, and complex deterministic seasonality (Figure 1). The trend pattern is a long-term evolution in the data, it can be increasing or decreasing, and it can have different forms (linear, exponential and damped) (Montgomery et al. 2015). An increasing trend can appear in the demand for technologies in the social fields, while a decreasing trend is related to epidemics, mortality rates, and unemployment (Parmezan et al. 2019). The seasonality pattern can be described as the occurrence of short-term regular variation that repeats at known and relatively constant time intervals. This type of patterns can occur in different types of data including time series of sales, e.g., the increase in sales of warm clothing in winter and air conditioners in summer (Parmezan et al. 2019).
2. Random-Walk behavior. The time series of this behavior are characterized by the existence of unit-root patterns. This behavior appears when the time series have a stochastic increasing or decreasing trend and/or stochastic seasonality (Figure 2). Here the current observation is equal to the previous observation plus a random step. The lag between these two observations is equal to one in the case of trend, and equal to the seasonality period in the case of seasonality.

The presence of deterministic or random-walk behavior induce the non-stationarity in time series. The stationarity is a relevant feature in time series which basically implies that the mean, the variance, and the covariance do not depend on time (Montgomery et al. 2015). These two types of behaviors are the most important features in time series, and usually characterize business and macro-economic data (Salles et al. 2019, Liu et al. 2019).

3. Nonlinear behavior. Time series observations can often exhibit correlations with different degrees of non-linearity (Figure 3). This type of behavior is present in almost all real-world time series data, such as in stream-flow forecasting (Wang et al. 2020), and in financial markets forecasting (Bukhari et al. 2020).
4. Long-memory behavior. Some time series may present properties of long-range dependencies in time which implies strong coupling effect between the values of observations at different time steps, i.e. the correlations between observations has a slower exponential decay compared to short range dependencies (Figure 4). This type of behavior can occur in hydrology forecasting (Papacharalampous and Tyrallis 2020), network traffic forecasting (Ramakrishnan and Soni 2018), financial market forecasting (Bukhari et al. 2020), etc.

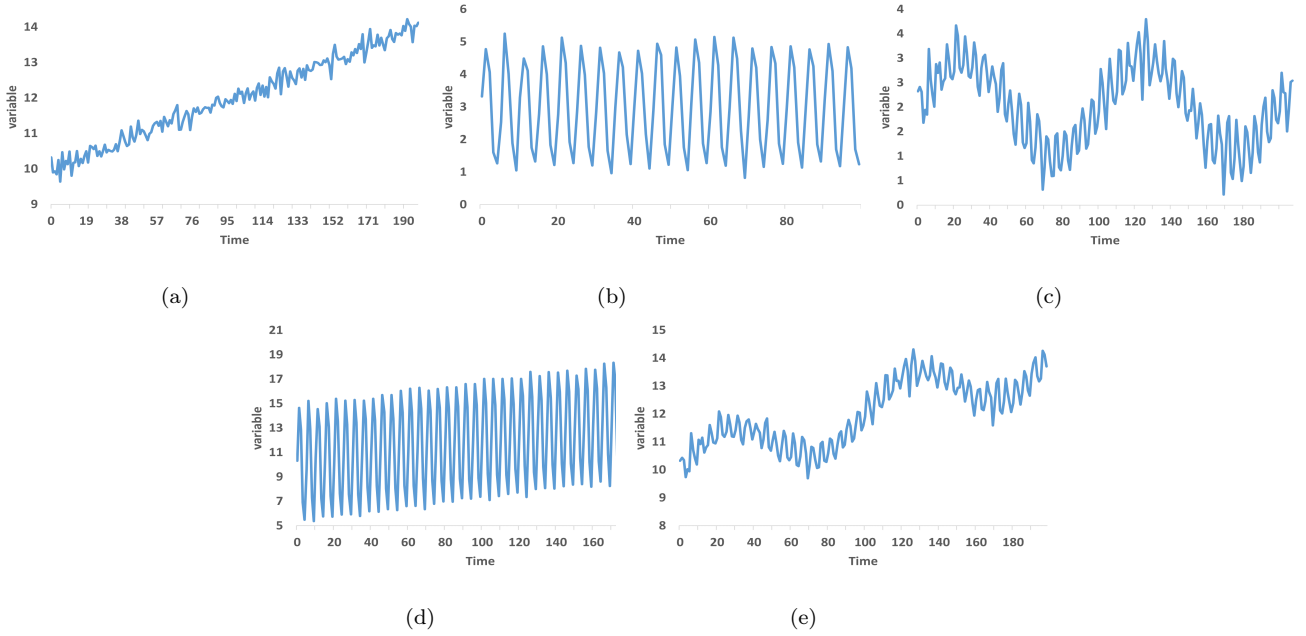


Figure 1: Time series with deterministic behavior: (a) increasing trend, (b) simple seasonality, (c) complex seasonality, (d) increasing trend and simple seasonality and (e) increasing trend and complex seasonality.

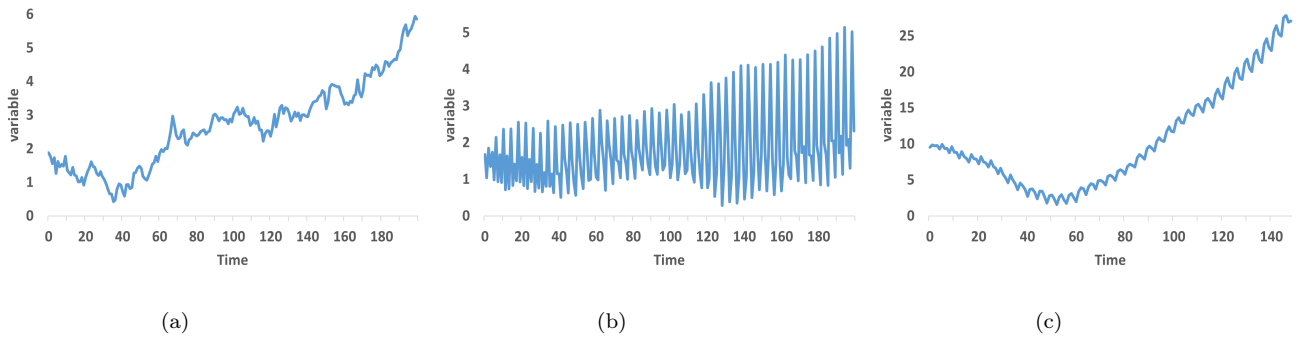


Figure 2: Time series with random-walk behavior: (a) trend random-walk, (b) seasonal random-walk, (c) trend and seasonal random-walk.

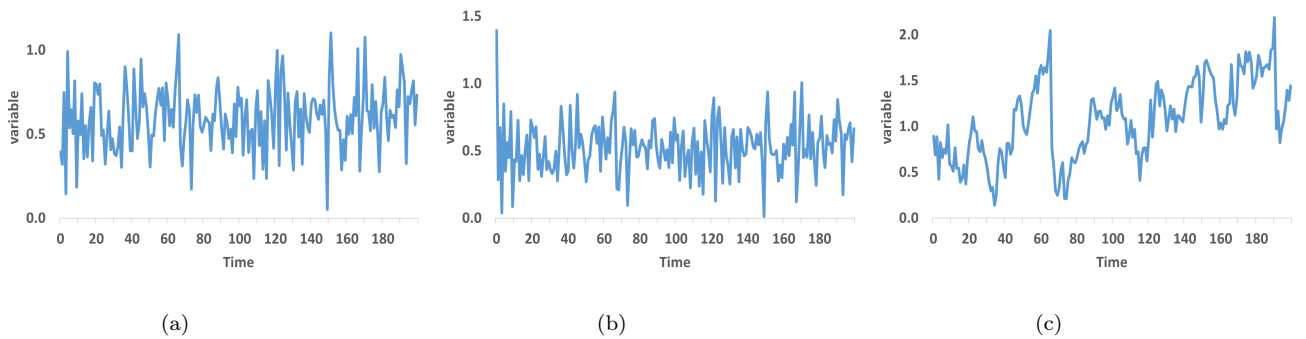


Figure 3: Time series with nonlinear behavior generated by: (a) Nonlinear Auto-Regressive (NAR) process, (b) Smooth Transition Auto-Regressive (STAR) process, (c) Threshold Auto-Regressive (TAR) process.

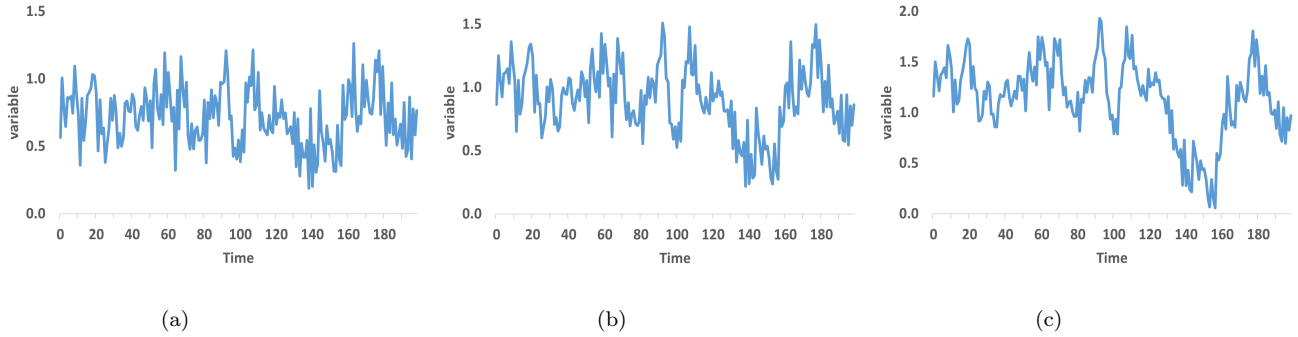


Figure 4: Time series with long-memory behavior: (a) short memory generated by ARFIMA(2,0.0,2), (b) long memory generated by ARFIMA(2,0.2,2) and (c) long memory generated by ARFIMA(2,0.4,2).

3.2. Chaotic behavior

The chaotic mechanism can be expressed as a nonlinear deterministic dynamical system that is often unknown or incompletely understood (Li and Lin 2016), real time series can exhibit a noisy chaotic behavior (Figure 5). These time series are sensitive to initial conditions (butterfly effect) where a small smooth perturbations in the system or measurement errors generate an abrupt change in the behavior of the time series (bifurcation). This type of behaviors is unstable since it tends to be deterministic at short term but random at long term. Such kind of time series are usually present in many science and engineering fields such as weather forecasting (Tian 2019), financial markets forecasting (Bukhari et al. 2020), energy forecasting (Bourdeau et al. 2019), intelligent transport and trajectory forecasting (Giuliani et al. 2021), etc.

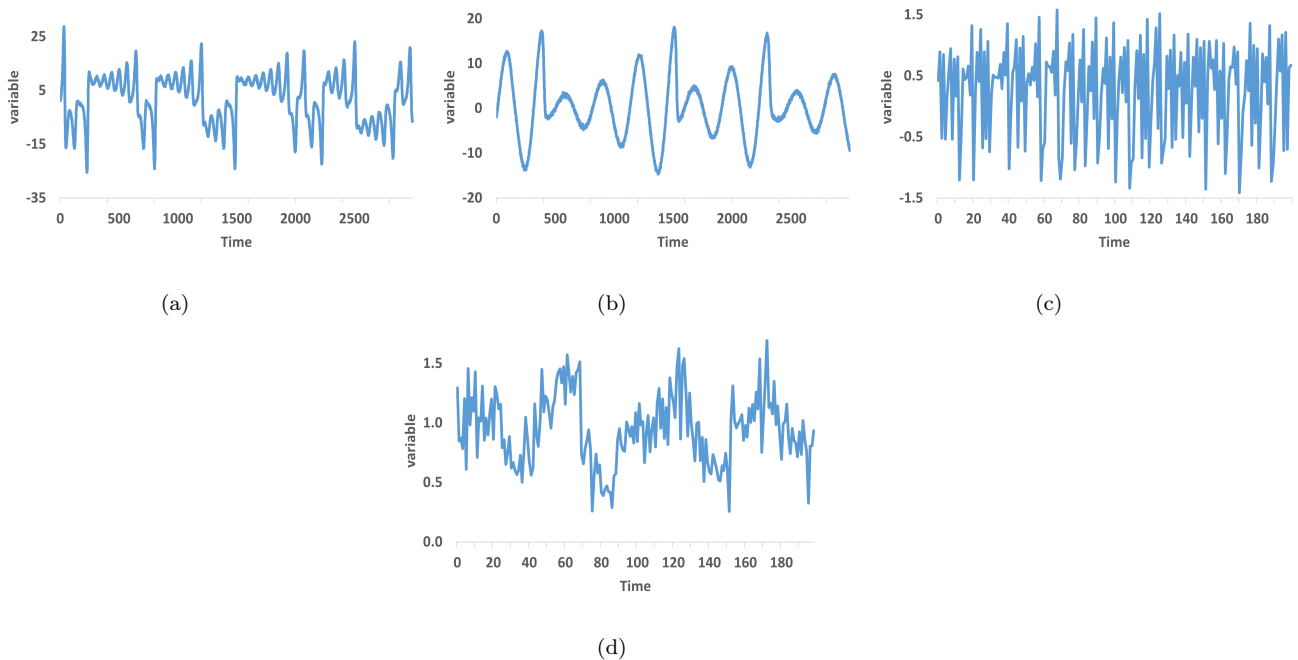


Figure 5: Time series with noisy chaotic behavior: (a) TS generated by Lorenz process. (b) TS generated by Rössler process. (c) TS generated by Hénon map process. (d) TS generated by Mackey-Glass process.

Based on the literature (Chandra and Zhang 2012, Montgomery et al. 2015, Liu et al. 2017, Fischer et al. 2018), the five aforementioned behaviors (deterministic, random-walk, nonlinear, long-memory, and chaotic) are the main behaviors encountered in real applications. Real-world time series can either express an individual behavior or an aggregation of more than one behavior. To identify which type of behavior a real-world time series can include, different statistical preprocessing tools and tests can be applied (Grau-Carles 2005, Inglada-Perez 2020). In Table 1, we present a set of tools that can be used to identify the existence of the five aforementioned behaviors in the time series data.

Table 1: A set of tools used to identify the five different time series behaviors.

Tool	Time series behavior	Reference
Data visualization	Deterministic behavior	Chatfield (2013)
Correlogram	Deterministic behavior	Box et al. (2015)
Time series decomposition	Deterministic behavior	Chatfield (2013)
Smoothing	Deterministic behavior	Montgomery et al. (2015)
Data visualization	Random-Walk behavior	Montgomery et al. (2015)
Augmented Dickey Fuller (ADF) test	Random-Walk behavior	Dickey and Fuller (1979)
Phillips–Perron (PP) test	Random-Walk behavior	Phillips and Perron (1988)
Kwiatkowski–Phillips–Schmidt–Shin (KPSS) test	Random-Walk behavior	Kwiatkowski et al. (1992)
Kaplan test	Nonlinear behavior	Kaplan (1994)
Keenan test	Nonlinear behavior	Keenan (1985)
Tsay test	Nonlinear behavior	Tsay (1986)
Teräsvirta test	Nonlinear behavior	Teräsvirta et al. (1993)
White test	Nonlinear behavior	White (1989)
Correlogram	Long-memory behavior	Palma (2007)
Qu test	Long-memory behavior	Qu (2011)
R/S analysis	Long-memory behavior	Mandelbrot and Wallis (1968)
Modified R/S	Long-memory behavior	Lo (1991)
Geweke and Porter-Hudak (GPH) test	Long-memory behavior	Geweke and Porter-Hudak (1983)
Detrended Fluctuation Analysis (DFA)	Long-memory behavior	Peng et al. (1994)
Correlation Dimension	Chaotic behavior	Grassberger and Procaccia (1984)
Lyapunov Exponent	Chaotic behavior	Bensaïda and Litimi (2013)
MGRM test	Chaotic behavior	Matilla-García and Marín (2010)
Recurrence Plots	Chaotic behavior	Eckmann and Ruelle (1985)
0/1 test	Chaotic behavior	Gottwald and Melbourne (2004)

4. Taxonomy of RNN cells

Humans do not start their thinking from zero every second, our thoughts have persistence in the memory of our brains. For example, as the reader reads this paper, he/she understands each word based on his/her understanding of the words before. The absence of memory is the major shortcoming in traditional machine learning models, particularly in feed-forward neural networks (FNNs). To overcome this limitation, RNNs integrate the concept of feedback connections in their structure (Figure 6, where x_t and h_t are the input state and the hidden state at time step t , respectively). This mechanism enables RNNs to have a certain memory capable of capturing the dynamics in sequential data by conveying information through time.

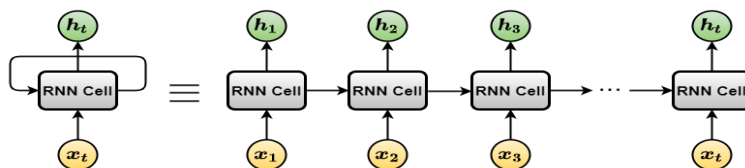


Figure 6: The folded (left) and unfolded (right) architecture of RNN model.

Table 2: A collection of RNN cell structures historically sorted.

RNN cell structure	Year	Reference
JORDAN	1989	Jordan (1989)
ELMAN	1990	Elman (1990)
LSTM-NFG	1997	Hochreiter and Schmidhuber (1997)
LSTM-Vanilla	2000	Gers et al. (2000)
LSTM-PC	2000	Gers and Schmidhuber (2000)
SCRN	2014	Mikolov et al. (2014)
GRU	2014	Cho et al. (2014)
IRNN	2015	Le et al. (2015)
LSTM-FB1	2015	Jozefowicz et al. (2015)
MUT	2015	Jozefowicz et al. (2015)
LSTM-CIFG	2015	Nina and Rodriguez (2015)
Differential LSTM	2015	Veeriah et al. (2015)
MRNN	2016	Abdulkarim (2016)
MGU	2016	Zhou et al. (2016)
Phased LSTM	2016	Neil et al. (2016)
Highway Connections	2016	Irie et al. (2016)
LSTM with Working Memory	2017	Pulver and Lyu (2017)
SLIM	2017	Lu and Salem (2017), Dey and Salem (2017), Heck and Salem (2017)
GORO	2019	Jing et al. (2019)

RNN models are built based on one specific cell structure which is the core of all computations that occur in the network. Multiple cell structures have been created since 1989 (Table 2). The early cell structure is named JORDAN (Jordan 1989), where at each time step the previous output state is fed into the cell (Figure 7a). Later, ELMAN cell was proposed by Elman (1990). Unlike the JORDAN cell, each time step in the ELMAN cell calls the previous hidden state (Figure 7b). In 2016, a combination of both JORDAN and ELMAN cells in one cell named multi-recurrent neural network (MRNN) was evaluated by Abdulkarim (2016). In this cell structure, at each time step, both previous output and hidden states are presented to the cell (Figure 7c).

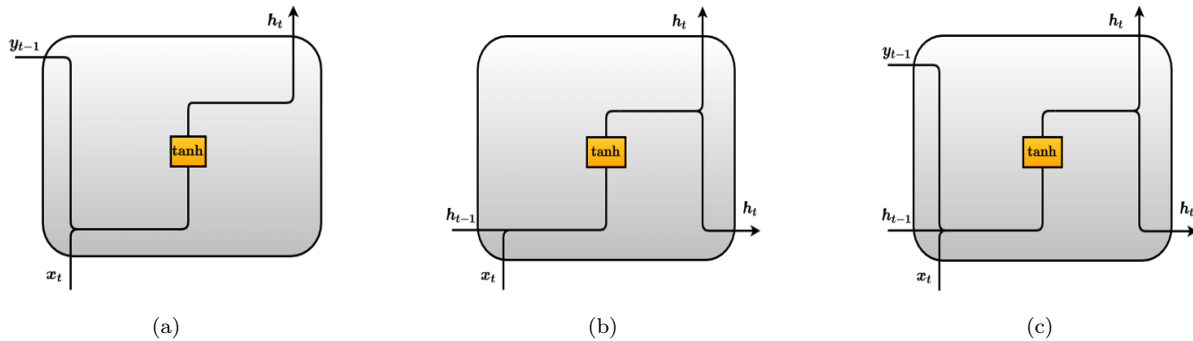


Figure 7: (a) JORDAN cell structure. (b) ELMAN cell structure. (c) MRNN cell structure.

It was proved that the ELMAN cell suffers from the vanishing and exploding gradient problems which impedes the capturing of long term dependencies (Pascanu et al. 2013). To overcome the memory limitation of this cell, novel cell structures have been proposed. In 2014, the Structurally Constrained Recurrent Network (SCRN) was proposed by Mikolov et al. (2014). They integrated a slight structural modification in ELMAN cell that consists in adding a new slowly changing state at each time step called context state s_{t-1} (Figure 8a). In 2015, Le et al. (2015) created a new cell called Identity Recurrent Neural Network (IRNN) as a modification of ELMAN by setting the ReLu as activation function, the identity matrix as an initialization of the hidden states weight matrix, and zero as an initialization of the bias (Figure 8b).

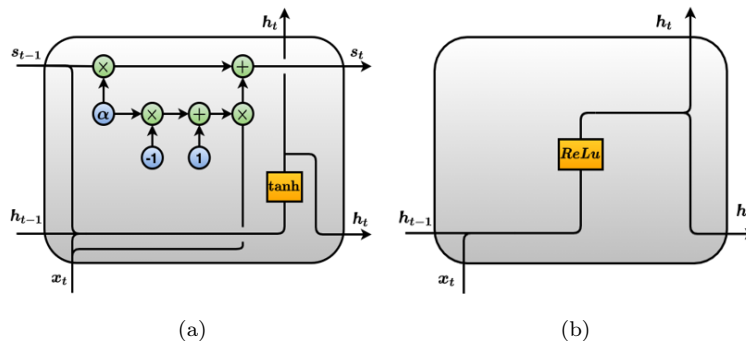


Figure 8: (a) SCRN cell structure. (b) IRNN cell structure.

A different way to handle the vanishing and exploding gradient problems resulted in creating different cell structures characterized by the gating mechanism that regulate the flowing of the information flux. The gates can be seen as filters that only hold useful information and selectively remove any irrelevant information from passing through. To perform this control of information (i.e., which information to pass and which information to discard), the gates are equipped with parameters that need to be trained through the model learning process using the back-propagation through time algorithm (Werbos 1990). Thus, this mechanism provides the RNN cell with an internal permanent memory able to store information for long time periods (Weston et al. 2014, Graves et al. 2014).

In 1997, the first version of this type of cells named Long-Short Term Memory with No Forget Gate (LSTM-NFG) was created by Hochreiter and Schmidhuber (1997). This cell contains two gates: the input gate Γ_{i_t} and the output gate Γ_{o_t} . Later in 2000, the concept of the forget gate Γ_{f_t} was introduced by Gers et al. (2000) creating LSTM-Vanilla that has been widely used in most applications (Figure 9a). In the same year, LSTM cell with peephole connections (LSTM-PC) was proposed by Gers and Schmidhuber (2000). The peephole connections connect the previous cell state c_{t-1} with the input, forget, and the output gates (Figure 9b). These connections enable the LSTM cell to inspect its current cell states (Gers and Schmidhuber 2001), and to learn precise and stable timing without teacher forcing (Gers et al. 2002).

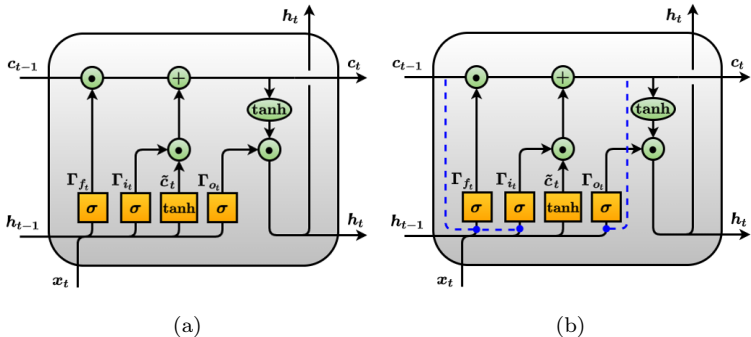


Figure 9: (a) LSTM-Vanilla cell structure. (b) LSTM-PC cell structure.

In 2014, Gated Recurrent Unit (GRU) was proposed by Cho et al. (2014) as a simpler variant of LSTM that shares many of the same properties. The idea behind GRU cell was to reduce the gating mechanism of LSTM cell from three gates to two gates (relevance gate Γ_{r_t} and update gate Γ_{u_t}) in order to decrease the number of parameters and to improve the learning velocity (Figure 10a). In 2015, ten thousand RNN cell structures were evaluated by Jozefowicz et al. (2015) using a mutation-based search process. They identified a cell architecture that outperforms both LSTM and GRU on some tasks. This cell consists in adding a bias of 1 to the LSTM forget gate creating LSTM-FB1. Further, they discovered three optimal cell architectures named MUT1, MUT2, and MUT3 that are similar to GRU but have some modifications in their gating mechanism and in their candidate hidden state \tilde{h}_t (Figure 10b and 10c). During that year, coupling both the input and the forget gates into one gate was proposed by Nina and Rodriguez (2015) creating LSTM-CIFG cell (Figure 11a). Further, the differential LSTM was proposed by Veeriah et al. (2015) to solve the impact

of spatial-temporal dynamics by introducing the differential gating scheme in LSTM cell.

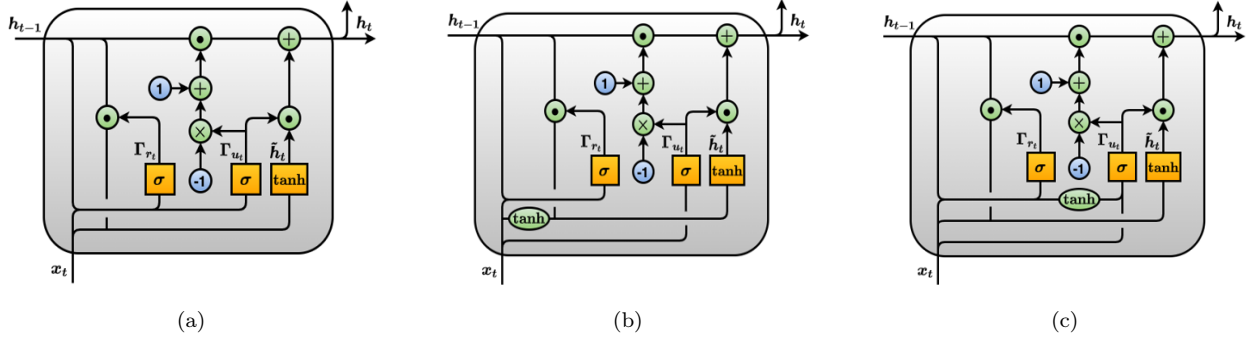


Figure 10: (a) GRU cell structure. (b) MUT1 cell structure. (c) MUT3 cell structure.

In 2016, the Minimal Gate Unit (MGU) cell was created by Zhou et al. (2016) to further reduce the number of parameters by decreasing the gating mechanism to one forget gate. This variant has simpler structure and fewer parameters compared to LSTM cell and GRU cell (Figure 11b). In the same year, eight variants of LSTM-PC (based on modifying, adding, or removing one cell component at each time) were evaluated by Greff et al. (2016) on three different types of task: speech recognition, polyphonic music modeling, and handwritten recognition. They demonstrated that the forget and the output gates are the most critical components in the LSTM cell. In addition, their results show that none of the evaluated variants can overcome the LSTM-PC cell. During that year, phased LSTM cell was introduced by Neil et al. (2016), where they added a time gate which updates the cell sparsely, and makes it converge faster than the basic LSTM. Further, highway connections were added to GRU and LSTM cells by Irie et al. (2016). In 2017, LSTM with working memory was created by Pulver and Lyu (2017), where they substituted the forget gate with a functional layer whose input depends on the previous cell state. In 2019, a Gated Orthogonal Recurrent Unit (GORO) was introduced by Jing et al. (2019), where they added to the GRU cell an orthogonal matrix that replaced the hidden state loop matrix.

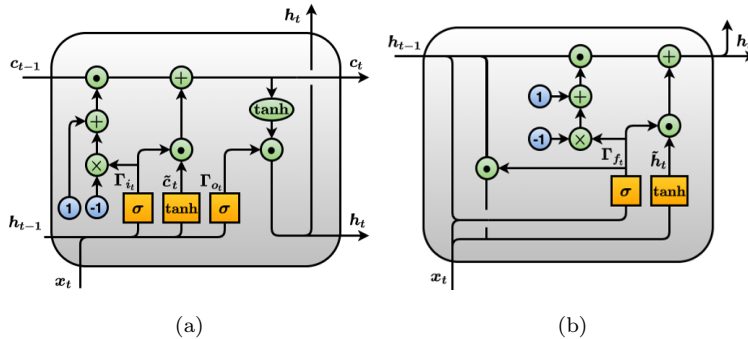


Figure 11: (a) LSTM-CIFG cell structure. (b) MGU cell structure.

While very powerful in long term dependencies, the basic cells (LSTM, GRU, and MGU) have complex structure with relatively large number of parameters. In 2017, the concept of parameter reduction was differently tackled through the creation of new cells called SLIM (Lu and Salem 2017, Dey and Salem 2017, Heck and Salem 2017). These variants aim to reduce aggressively the parameters in order to achieve memory and time savings while necessarily retaining a performance comparable to the basic cells. The new parameter-reduced variants of these cells eliminate the combinations of the input state, the hidden state, and the bias from the individual gating signals, creating SLIM1, SLIM2, and SLIM3, respectively. The SLIM1 cell consists in removing from the mechanism of all the gates the input state and its associated parameter matrix (Figure 12a). SLIM2 cell consists in maintaining only the hidden state and its associated parameter matrix (Figure 12b). Whereas, SLIM3 cell consists in removing the input state, the hidden state, and their associated parameters matrices (Figure 12c). The cellular calculations within the displayed RNN cells along with the evaluated ones are provided in Appendix.

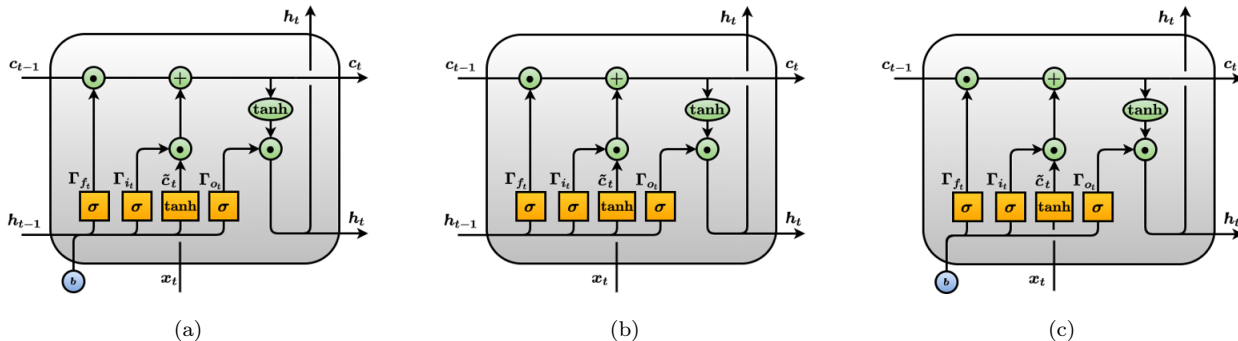


Figure 12: (a) SLIM1 cell structure. (b) SLIM2 cell structure. (c) SLIM3 cell structure.

5. Experimental structure

Two experiments have been carried out in this study. The first experiment analyzes the utility of each LSTM-Vanilla cell component in forecasting time series behaviors. The second experiment evaluates different variants of RNN cell structures in forecasting time series behaviors. In this section, we first describe the process we followed to generate the dataset for each time series behavior (Section 5.1). Then, we present the selected models for the first and second experiment (Section 5.2). Finally, we provide the setup of the used models (Section 5.3).

5.1. Synthetic data generation

To simulate the five aforementioned time series behaviors, we used 21 different DGPs with white Gaussian noise $\epsilon_t \sim \mathcal{N}(\mu = 0, \sigma = 0.2)$. From each DGP we created time series of length 3000 observations replicated 30 times through a Monte Carlo simulation experiment using different initial random seeds for the white noise term ϵ_t (Table 3).

To generate time series with deterministic behavior, 5 DGPs were used (Table 4): Trend process (T), Simple Seasonality process (SS), Complex Seasonality process (CS), Trend and Simple Seasonality process

(TSS), and Trend and Complex Seasonality process (TCS). To simulate the random-walk behavior, 3 DGPs were used (Table 5): Trend Random-Walk process (TRW), Seasonal Random-Walk process (SRW), and Trend and Seasonal Random-Walk process (TSRW). To simulate time series with nonlinear behavior, we used 6 most popular nonlinear models commonly used in the forecasting literature having an increasing levels of non-linearity (Zhang et al. 2001) (Table 6): Sign Auto-Regressive process (SAR), Nonlinear Moving Average process (NMA), Nonlinear Auto-Regressive process (NAR), Bilinear process (BL), Smooth Transition Auto-Regressive process (STAR), and Threshold Auto-Regressive process (TAR). These models are motivated by many nonlinear characteristics commonly observed in practice. To artificially generate time series with long memory behavior, we used the Auto-Regressive Fractionally Integrated Moving Average process ARFIMA(p,d,q) since it is one of the best-known long memory processes (Liu et al. 2017). In order to evaluate the performance of RNN cell structures with respect to DGPs with an increasing memory structure, 3 DGPs were created based on the variation of the fractional order of ARFIMA process $d = \{0, 0.2, 0.4\}$. A higher fractional order d implies longer dependency structure (Table 7). To ensure the stationarity of the generated time series, we set the values of the fractional order strictly less than 0.5. Finally, to simulate the noisy chaotic behavior, 4 most known chaotic DGPs were used (Table 8): Mackey-Glass process, Lorenz process, Rössler process, and Hénon-Map process. Then, we added the white Gaussian noise ϵ_t to the deterministic signals to create noisy chaotic time series (Sangiorgio et al. 2021).

Table 3: Number of data generation processes and time series in each behavior.

Behavior	# DGPs	# Time series
Deterministic behavior	5	150
Random-walk behavior	3	90
Nonlinear behavior	6	180
Long-memory behavior	2	60
Chaotic behavior	4	120
Total	21	600

Table 4: The DGPs used to simulate time series with deterministic behavior.

Process name	Process mathematical model
Trend process	$(T) : z_t = 10 + 0.02t + \epsilon_t$
Simple Seasonality process	$(SS) : z_t = 2 \sin(2\pi t/5) + \epsilon_t$
Complex Seasonality process	$(CS) : z_t = \sin(2\pi t/100) + 0.5 \sin(2\pi t/5) + \epsilon_t$
Trend and Simple Seasonality process	$(TSS) : z_t = 10 + 0.02t + 5 \sin(2\pi t/5) + \epsilon_t$
Trend and Complex Seasonality process	$(TCS) : z_t = 10 + 0.02t + \sin(2\pi t/100) + 0.5 \sin(2\pi t/5) + \epsilon_t$

Table 5: The DGPs used to simulate time series with random-walk behavior.

Process name	Process mathematical model
Trend Random-Walk process	$(TRW) : z_t = z_{t-1} + \epsilon_t$
Seasonal Random-Walk process	$(SRW) : z_t = z_{t-4} + \epsilon_t$
Trend and Seasonal Random-Walk process	$(TSRW) : z_t = z_{t-1} + z_{t-4} - z_{t-5} + \epsilon_t$

Table 6: The DGPs used to simulate time series with nonlinear behavior.

Process name	Process mathematical model
Sign Auto-Regressive process	$SAR(2) : z_t = sign(z_{t-1} + z_{t-2}) + \epsilon_t$ $sign(x) = \begin{cases} 1 & \text{if } x > 0 \\ 0 & \text{for } x = 0 \\ -1 & \text{for } x < 0 \end{cases}$
Nonlinear Moving Average process	$NMA(2) : z_t = \epsilon_t - 0.3\epsilon_{t-1} + 0.2\epsilon_{t-2} + 0.4\epsilon_{t-1}\epsilon_{t-2} - 0.25\epsilon_{t-2}^2$
Nonlinear Auto-Regressive process	$NAR(2) : z_t = \frac{0.7 z_{t-1} }{ z_{t-1} +2} + \frac{0.35 z_{t-2} }{ z_{t-2} +2} + \epsilon_t$
Bilinear process	$BL(2) : z_t = 0.4z_{t-1} - 0.3z_{t-2} + 0.5z_{t-1}\epsilon_{t-1} + \epsilon_t$
Smooth Transition Auto-Regressive process	$STAR(2) : z_t = 0.3z_{t-1} + 0.6z_{t-2} + \frac{0.1-0.9z_{t-1}+0.8z_{t-2}}{1+e^{-10z_{t-1}}} + \epsilon_t$
Threshold Auto-Regressive process	$TAR(2) : z_t = \begin{cases} 0.9z_{t-1} + 0.05z_{t-2} + \epsilon_t & \text{for } z_{t-1} \leq 1 \\ -0.3z_{t-1} + 0.65z_{t-2} - \epsilon_t & \text{for } z_{t-1} > 1 \end{cases}$

Table 7: The DGPs used to simulate time series with long-memory behavior.

Process name	Process mathematical model
$ARFIMA(p = 2, d = 0.0, q = 2)$	$z_t^{(0.0)} = 0.7z_{t-1}^{(0.0)} - 0.1z_{t-2}^{(0.0)} - 0.5\epsilon_{t-1} + 0.4\epsilon_{t-2} + \epsilon_t$
$ARFIMA(p = 2, d = 0.2, q = 2)$	$z_t^{(0.2)} = 0.7z_{t-1}^{(0.2)} - 0.1z_{t-2}^{(0.2)} - 0.5\epsilon_{t-1} + 0.4\epsilon_{t-2} + \epsilon_t$
$ARFIMA(p = 2, d = 0.4, q = 2)$	$z_t^{(0.4)} = 0.7z_{t-1}^{(0.4)} - 0.1z_{t-2}^{(0.4)} - 0.5\epsilon_{t-1} + 0.4\epsilon_{t-2} + \epsilon_t$

Table 8: The DGPs used to simulate time series with chaotic behavior.

Process name	Process mathematical model
Mackey-Glass process	$\frac{dx}{dt} = a \frac{x(t-\pi)}{1+x^c(t-\pi)} - bx(t)$ such that $(\tau = 17, a = 0.2, b = 0.1, c = 10)$ (Ma et al. 2007)
Hénon-Map process	$x_{t+1} = 1 + y_t - ax_t^2 ; y_{t+1} = bx_t$ such that $(a = 1.4, b = 0.3)$ (Li and Lin 2016)
Rössler process	$\dot{x} = -y - z ; \dot{y} = x + ay ; \dot{z} = b + z(x - c)$ $(a = 0.15, b = 0.2, c = 10, x_0 = 10, y_0 = z_0 = 0)$ (Lim and Puthusserypady 2007)
Lorenz process	$\dot{x} = \sigma(y - x) ; \dot{y} = -xz + rx - y ; \dot{z} = xy - bz$ $(\sigma = 16, r = 45.92, b = 4, x_0 = y_0 = z_0 = 1)$ (Lim and Puthusserypady 2007)

5.2. RNN-cells used for experiment 1 and 2

To evaluate each cell structure with respect to each times series behavior, we conducted two experiments as summarized in Table 9. The first experiment evaluates LSTM-Vanilla and 11 of its variants created based on one alteration in the basic Vanilla architecture that consists of (1) removing, (2) adding, or (3) substituting one cell component (Table A.16): (1) The first three variants NIG (No Input Gate), NFG (No Forget Gate), and NOG (No Output Gate) were created through the deactivation of the input gate, the forget gate, and the output gate, respectively. The four subsequent variants NIAF (No Input Activation Function), NFAF (No Forget Activation Function), NOAF (No Output Activation Function), and NCAF (No Candidate Activation Function) were constructed through the elimination of the input, forget, output, and candidate activation function, respectively. (2) The two subsequent variants PC (Peephole Connections), and FGR (Full Gate Recurrence) were designed through the creation of new connections between the cell state and the gates, and between the current states and the previous states of the gates, respectively. (3) Eventually, FB1 (Forget Gate Bias 1) and CIFG (Coupled Input Forget Gate) were conceived by setting the forget gate bias to one, and by coupling the input and the forget gate into one gate, respectively.

The second experiment evaluates and analyzes the performance of 20 possible RNN-cell structures: JORDAN, ELMAN, MRNN, SCRNN, IRNN, LSTM-Vanilla, GRU, MGU, MUT1, MUT2, MUT3, and 9 SLIM variants mapping LSTM, GRU, and MGU. A summary of the evaluated cells related to each experiment is presented in Table 9, and the cellular calculations inside each cell is presented in Table A.17.

The studied RNN cells have different degrees of complexity, which is referred to as theoretic complexity. This complexity is defined by the number of parameters inside each cell which depends on the number of inputs, the number of hidden nodes, the number of context nodes (in the case of SCRNN model), and the number of outputs. During the hyper-parameter tuning the complexity of the cell may increase or decrease depending on the optimal number of hidden nodes found. Thus, the complexity of the cell defined after the hyper-parameter tuning is called empirical complexity.

5.3. Experimental setup

Before starting the modeling process, each time series data was partitioned into three subsets: the first 2000 observations were used to train the models in order to find the best parameters, the next 500 observations were used to select the best configuration of each model, and the last 500 observations were used to test the out-of-sample performance of these models. Each partition was normalized, then reshaped using the estimation window size (number of lags) and the forecasting window size (number of horizons) to convert them into supervised learning data (input-target). To find the best configuration of the studied models, we fixed some hyper-parameters (Table 13) and varied other ones. The process of hyper-parameter optimization consists in finding the best number of hidden neurons and the best estimation window size using the Grid Search algorithm. The ranges of values used to find the best estimation window size for each DGP are presented in Table 11. Each model’s configuration (combination of number of hidden nodes and estimation window size) was run 10 times to test its performance stability.

Table 9: List of evaluated RNN models with regard to each experiment with their theoretic complexity, number of weight matrices, and number of bias vectors. n_I is the number of inputs, n_H is the number of hidden nodes, n_S is the number of context nodes, and n_O is the number outputs.

		RNN models				
	Short name	Full name	Theoretic complexity	# Weight matrices	# Bias vectors	
Experiment 1	NIG	LSTM with No Input Gate	$3n_I n_H + 3n_H^2 + 3n_H$	6	3	
	NFG	LSTM with No Forget Gate	$3n_I n_H + 3n_H^2 + 3n_H$	6	3	
	NOG	LSTM with No Output Gate	$3n_I n_H + 3n_H^2 + 3n_H$	6	3	
	CIFG	LSTM with Coupled Input Forget Gate	$3n_I n_H + 3n_H^2 + 3n_H$	6	3	
	FB1	LSTM with Forget Gate Bias 1	$4n_I n_H + 4n_H^2 + 3n_H$	6	3	
	NIAF	LSTM with No Input Activation Function	$4n_I n_H + 4n_H^2 + 4n_H$	8	4	
	NFAF	LSTM with No Forget Activation Function	$4n_I n_H + 4n_H^2 + 4n_H$	8	4	
	NOAF	LSTM with No Output Activation Function	$4n_I n_H + 4n_H^2 + 4n_H$	8	4	
	NCAF	LSTM with No Candidate Activation Function	$4n_I n_H + 4n_H^2 + 4n_H$	8	4	
	Vanilla	LSTM Vanilla	$4n_I n_H + 4n_H^2 + 4n_H$	8	4	
	PC	LSTM with Peephole Connections	$4n_I n_H + 7n_H^2 + 4n_H$	11	4	
	FGR	LSTM with Full Gate Recurrence	$4n_I n_H + 13n_H^2 + 4n_H$	17	4	
	Experiment 2	ELMAN	ELMAN	$n_I n_H + n_H^2 + n_H$	2	1
		IRNN	Identity Recurrent Neural Network	$n_I n_H + n_H^2 + n_H$	2	1
JORDAN		JORDAN	$n_I n_H + n_O n_H + n_H$	2	1	
MRNN		Multi-Recurrent Neural Network	$n_I n_H + n_H^2 + n_O n_H + n_H$	3	1	
SCRN		Structurally Constrained Recurrent Network	$n_I n_S + n_I n_H + n_H^2 + n_S n_H + n_H$	4	1	
MGU-SLIM3		Minimal Gate Unit SLIM3	$n_I n_H + n_H^2 + 2n_H$	2	2	
MGU-SLIM2		Minimal Gate Unit SLIM2	$n_I n_H + 2n_H^2 + n_H$	3	1	
MGU-SLIM1		Minimal Gate Unit SLIM1	$n_I n_H + 2n_H^2 + 2n_H$	3	2	
MGU		Minimal Gate Unit	$2n_I n_H + 2n_H^2 + 2n_H$	4	2	
GRU-SLIM3		Gated Recurrent Unit SLIM3	$n_I n_H + n_H^2 + 3n_H$	2	3	
GRU-SLIM2		Gated Recurrent Unit SLIM2	$n_I n_H + 3n_H^2 + n_H$	4	1	
GRU-SLIM1		Gated Recurrent Unit SLIM1	$n_I n_H + 3n_H^2 + 3n_H$	4	3	
MUT1		Gated Recurrent Unit Mutation 1	$2n_I n_H + 2n_H^2 + 3n_H$	4	3	
MUT2		Gated Recurrent Unit Mutation 2	$2n_I n_H + 3n_H^2 + 3n_H$	5	3	
MUT3		Gated Recurrent Unit Mutation 3	$3n_I n_H + 3n_H^2 + 3n_H$	6	3	
GRU		Gated Recurrent Unit	$3n_I n_H + 3n_H^2 + 3n_H$	6	3	
LSTM-SLIM3		LSTM SLIM3	$n_I n_H + n_H^2 + 4n_H$	2	4	
LSTM-SLIM2		LSTM SLIM2	$n_I n_H + 4n_H^2 + n_H$	5	1	
LSTM-SLIM1		LSTM SLIM1	$n_I n_H + 4n_H^2 + 4n_H$	5	4	
LSTM-Vanilla		LSTM Vanilla	$4n_I n_H + 4n_H^2 + 4n_H$	8	4	

Table 10: The values of the hyper-parameters used to train the studied RNN models.

Hyper-parameter	Value
Mini-batch size	100
Maximum number of epochs	500
Initial learning rate	0.01
Learning algorithm	Adam
Forecasting window size (horizon)	1
Number of hidden neurons	(1:1:10)
	(initial: step: final)

Table 11: The range of values used as inputs for the studied RNN models with respect to the DGPs of each time series behavior.

Behavior	DGP	Estimation window size
Deterministic behavior	T	1:1:10
	SS	1:1:5
	CS	1:1:5
	TSS	1:1:5
	TCS	1:1:5
Random-walk behavior	TRW	1:1:10
	SRW	1:1:4
	TSRW	1:1:5
Nonlinear behavior	SAR(2)	1:1:5
	NMA(2)	1:1:5
	NAR(2)	1:1:5
	BL(2)	1:1:5
	STAR(2)	1:1:5
	TAR(2)	1:1:5
Long-memory behavior	ARFIMA(2, 0, 2)	1:1:5
	ARFIMA(2, 0.2, 2)	1:1:20
	ARFIMA(2, 0.4, 2)	1:1:40
Chaotic behavior	Mackey-Glass	1:1:7
	Hénon map	1:1:3
	Rössler	1:1:14
	Lorenz	1:1:25

Once finding the best configuration of each model, the training and the validations sets were blended to form a new training set on which these models were retrained on for 500 epochs. To evaluate the forecasting performance of the models the Root Mean Square Error (RMSE) was used:

$$RMSE = \sqrt{\frac{1}{n} \sum_{t=1}^n (y_t - \hat{y}_t)^2}$$

Where y_t and \hat{y}_t are the real value and the predicted value at time step t , respectively. And n is the number of observations in the time series. The predicted values are computed as:

$$\hat{y}_t = h_t \cdot W_{hy} + b_y$$

W_{hy} is the weight matrix between the hidden and the output layer, and b_y is the output layer bias.

6. Results and discussion

In this section, we present the results of the two conducted experiments: (1) The first experiment consists of evaluating and analyzing the role of each component in LSTM-Vanilla cell with respect to the five time series behaviors. The evaluated architectures were generated by removing (NIG, NFG, NOG, NIAF, NFAF, NOAF, and NCAF), adding (PC and FGR), or substituting (FB1 and CIFG) one cell component. (2) The second experiment aims at evaluating and analyzing the performance of all possible RNN cell structures (JORDAN, ELMAN, MRNN, SCRNN, IRNN, LSTM-Vanilla, GRU, MGU, MUT1, MUT2, MUT3, and 9 SLIM variants) in forecasting the five behaviors.

The RNN cells presented in the following figures are ordered based on their theoretic complexity in order to maintain the same order in all the figures of the five behaviors so as to facilitate their interpretation. To grab the reader’s attention to the best RNN cell within each DGP and within each behavior, we used the star symbol (i.e. \star and \star). Two colors were used so as to differentiate between models having the same forecasting errors but different empirical complexities. The symbol \star is used to highlight the model having the smallest forecasting error and the smallest empirical complexity. However, the symbol \star is used to highlight the model(s) having similar forecasting error(s) as the \star model but with a relatively higher empirical complexity compared to this one. In the case where more than one cell structure provide similar forecasting errors, the simplest architecture (i.e., the \star model) is recommended based on the principle of Occam’s Razor (Blumer et al. 1987).

6.1. Experiment 1: Utility analysis of LSTM cell components in forecasting time series behaviors.

The impact of each component (i.e., input gate, forget gate, output gate, coupled input-forget gate, input activation function, forget activation function, output activation function, candidate activation function, fixing the forget bias to 1, peephole connections, and full gate recurrence) on the performance of LSTM-Vanilla model for predicting the deterministic behavior, random-walk behavior, nonlinear behavior, long-memory behavior, and chaotic behavior is shown, respectively, in Figures 13, 14, 15, 16 and 17.

As it can be observed from Figure 13, for modeling time series with deterministic behavior, LSTM cell structures behave differently to each deterministic time series patterns (T, SS, CS, TSS, and TCS) (Figure 13). The forget and the candidate activation functions are the most relevant cell components in forecasting time series with TSS pattern. Substituting the forget gate bias with the value one deteriorates the cell forecasting ability towards time series with TSS pattern. The existence of the output gate is necessary in forecasting time series with SS pattern. In almost all models, forecasting the CS pattern is very challenging compared to the other patterns, while the T pattern is easily captured. To model time series with random-walk behavior, the input activation function is of paramount importance to capture the TSRW pattern. The

FGR variant outperforms in capturing the SRW pattern, however, its performance widely degrades with respect to TSRW pattern. Adding the peephole connections make the LSTM cell behave similarly to both patterns TRW and SRW. Whereas, coupling the input and the forget gates make the LSTM cell perform equally to SRW and TSRW patterns (Figure 14).

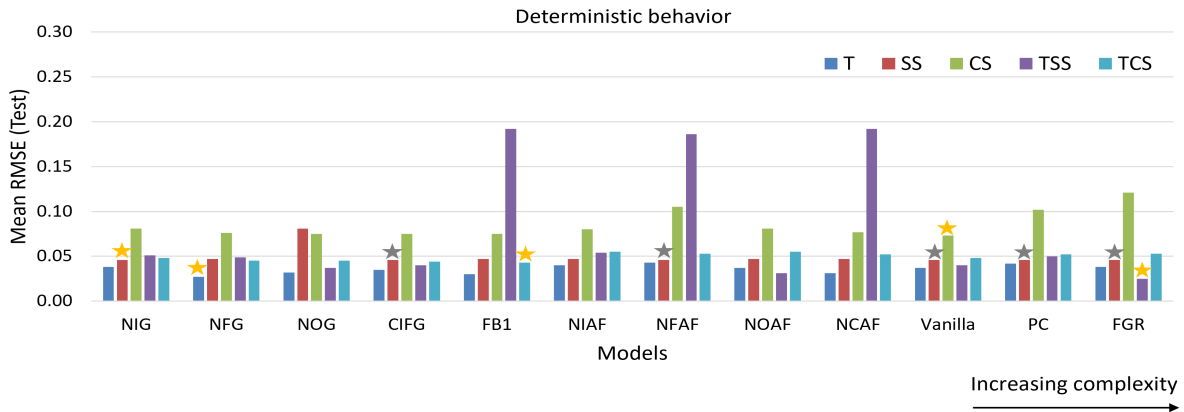


Figure 13: Forecasting performance of LSTM-Vanilla cell structures with respect to time series with deterministic behavior generated by 5 types of DGPs: T, SS, CS, TSS, and TCS.

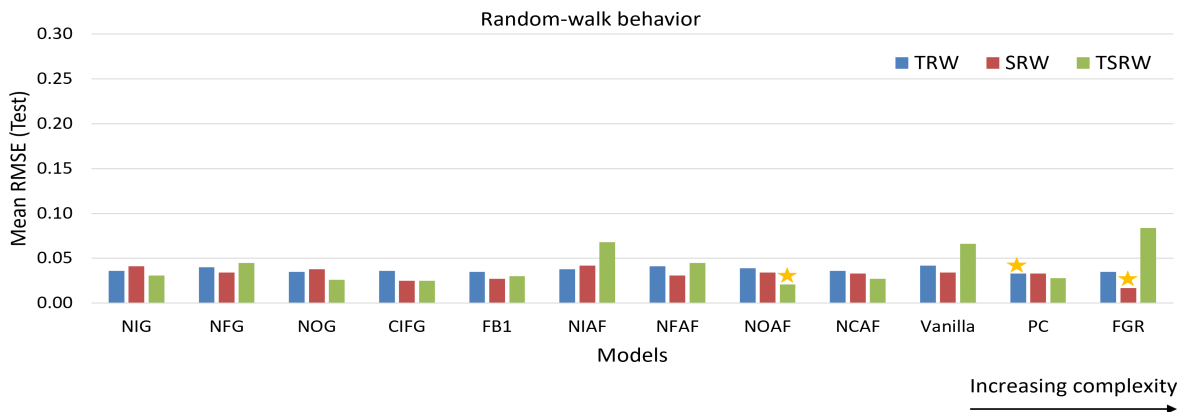


Figure 14: Forecasting performance of LSTM-Vanilla cell structures with respect to time series with random-walk behavior generated by 3 types of DGPs: TRW, SRW, and TSRW.

Regarding the nonlinear behavior, the LSTM structures behave similarly to all the 6 nonlinear time series patterns (Figure 15). Their errors decrease with the increase in the non-linearity order of the time series. This proves that all the components in the LSTM cell are able to capture the strong non-linearity in time series more than the soft non-linearity pattern. With regard to the long-memory behavior, the LSTM structures display approximately similar ability in forecasting the 3 long-memory degrees (Figure 16). Their errors decrease with the increase in the long memory order. Nevertheless, the NOAF cell exhibits a different

behavior. It presents a peak in the RMSE with respect to the highest long-memory degree. Therefore, the output activation function plays a major role in capturing the long range dependencies in time series data.

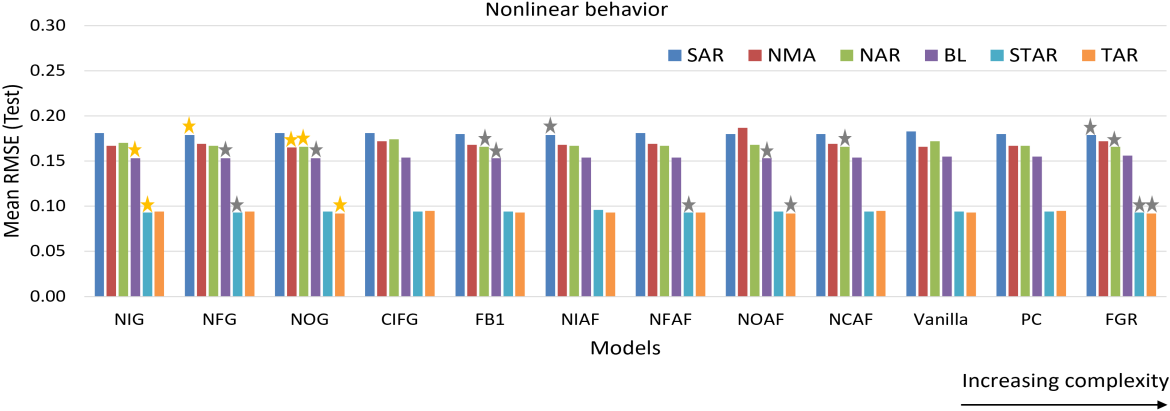


Figure 15: Forecasting performance of LSTM-Vanilla cell structures with respect to time series with nonlinear behavior generated by 6 types of DGPs: SAR(2), NMA(2), NAR(2), BL(2), STAR(2), and TAR(2).

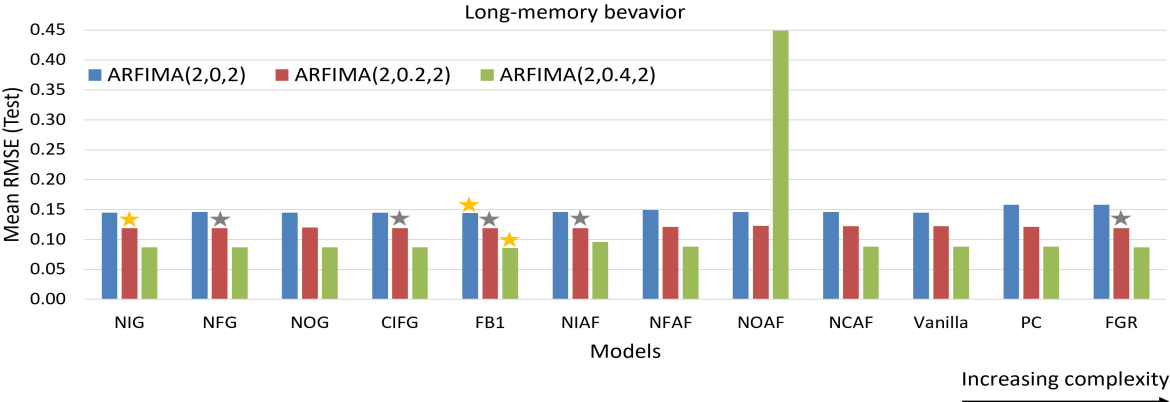


Figure 16: Forecasting performance of LSTM-Vanilla cell structures with respect to time series with long-memory behavior generated by 3 types of DGPs using ARFIMA with $d = \{0, 0.2, 0.4\}$.

Within the chaotic behavior, almost all the LSTM variants behave similarly to all the 4 chaotic behaviors (Figure 17). The Mackey-Glass process followed by the Hénon process are more challenging compared to the Rössler process followed by the Lorenz process. Although, with the NIAF, the FB1, and the PC variants, the forecasting error of the Hénon process exceeds the one of the Mackey-Glass process. The input and the forget activation functions are compulsory in modeling the Mackey-Glass process. The reasons that can degrade the forecasting performance of LSTM-vanilla cell with regard to the Hénon process are: removing the input activation function, coupling the input and the forget gates, substituting the forget gate bias by one, and adding the peephole connections.

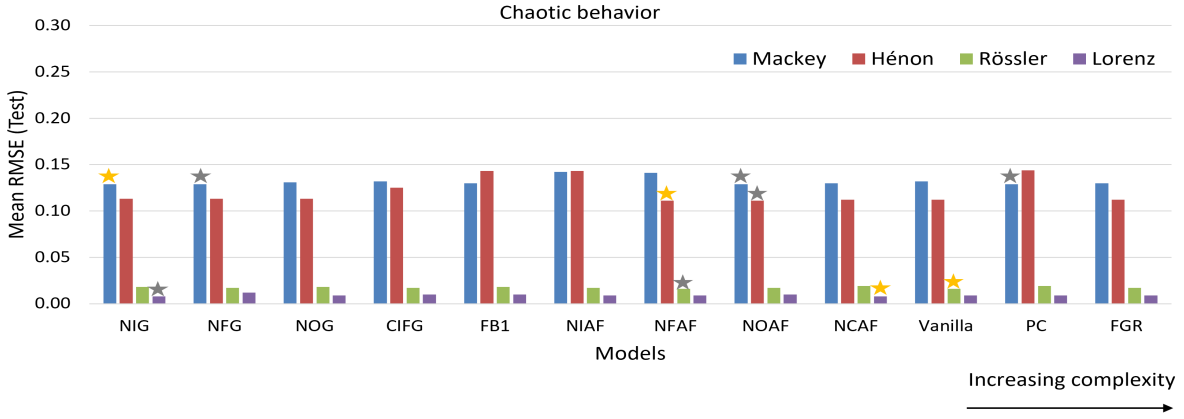


Figure 17: The test RMSE of different LSTM cell structures in forecasting time series with noisy chaotic behavior generated by 4 types of DGPs: Mackey-Glass , Lorenz, Rössler, and Hénon map.

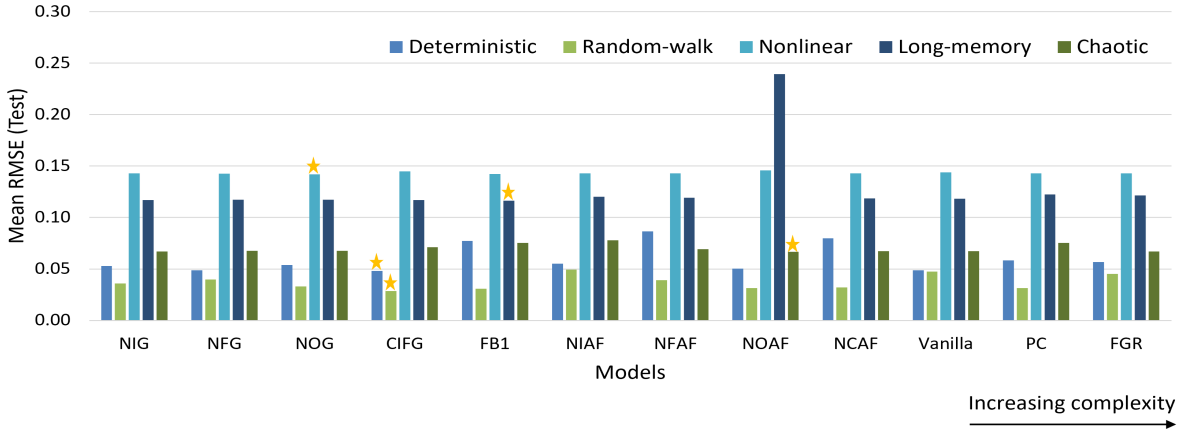


Figure 18: Average forecasting performance of each LSTM-Vanilla cell structure with respect to the five time series behaviors.

To identify the general forecasting ability of all the LSTM-vanilla variants for each time series behavior, we computed the mean RMSE over all the DGPs of each behavior (Figure 18). To capture the deterministic behavior, the CIFG model is the most recommended. The forget and the candidate activation functions are the most mandatory components in the LSTM cell. In addition, the bias of the forget gate should be set as a learnable parameter and not equal to one as in FB1. To model the random-walk behavior, the CIFG is the best model. The input activation function is very necessary, although, the Vanilla version of LSTM should be avoided. To model the nonlinear behavior, almost all the cell structures present similar performance, such that the NOG structure is the most recommended. To capture the long range dependencies in time series with long-memory behavior, the existence of the output activation function is very critical (i.e., when it is removed, the forecasting error gets multiplied by 2). Almost all the remaining LSTM structures present

similar results, however, the FB1 variant is the most performing. To model the chaotic behavior, all the LSTM structures have approximately the same performance, such that the NOAF structure is the most recommended. In Table 12, we provide guidelines about the best LSTM cell structure to be used in each process and in each time series behavior.

Table 12: Guidelines on the best LSTM cell structure for each time series behavior. The Mean refers to the best cell structure over all the DGPs of the same behavior. The two colored stars are used to differentiate between models with the same forecasting error but with different empirical complexity. (★) refers to model with the smallest forecasting error. (★) refers to model with the smallest forecasting error and empirical complexity.

Behaviors	DGPs	LSTM variants											
		NIG	NFG	NOG	CIFG	FB1	NIAF	NFAF	NOAF	NCAF	Vanilla	PC	FGR
Deterministic	T		★										
	SS	★			★			★			★	★	★
	CS										★		
	TSS												★
	TCS					★							
	Mean				★								
Unit-root	TRW											★	
	SRW												★
	TSRW								★				
	Mean				★								
Nonlinear	SAR(2)		★				★						★
	NMA(2)			★									
	NAR(2)			★		★				★			★
	BL(2)	★	★	★		★			★				
	STAR(2)	★	★					★					★
	TAR(2)			★					★				★
	Mean			★									
Long-memory	ARFIMA(2,0,2)									★			
	ARFIMA(2,0.2,2)	★	★		★	★	★						★
	ARFIMA(2,0.4,2)					★							
	Mean					★							
Chaotic	Mackey	★	★							★		★	
	Hénon							★	★				
	Rössler							★			★		
	Lorenz	★								★			
	Mean								★				

6.2. Experiment 2: Performance analysis of different RNN cell structures in forecasting time series behaviors.

The performance of each RNN cell structure (JORDAN, ELMAN, MRNN, SCRNN, IRNN, LSTM-Vanilla, GRU, MGU, MUT1, MUT2, MUT3, and 9 SLIM variants) for predicting the deterministic behavior, random-walk behavior, nonlinear behavior, long-memory behavior, and chaotic behavior is shown, respectively, in Figures 19, 20, 21, 22, and 23.

The RNN models behave similarly to the different deterministic time series patterns (Figure 19). Typically, for the majority of RNN cell structures, the CS pattern is the most challenging, while the T pattern is the less challenging. The simple recurrent cells (ELMAN, IRNN, JORDAN, MRNN, and SCRNN) and the MGU-SLIM1 cell are unable to model time series with TSS pattern because they exhibit a strong rise in the RMSE compared to the other models.

Regarding the random-walk behavior, the RNN models perform differently with respect to the different patterns (Figure 20). The models ELMAN, IRNN, JORDAN, and MRNN are unable to capture the TRW pattern since they depict an intense increase in the forecasting error. For the same pattern, MUT1 followed by SCRNN also depict a higher error compared to the remaining MGU, GRU, and LSTM variants. In addition, to model the SRW pattern, the MRNN model shows the highest error compared to all the other models. With respect to the three patterns, the SLIM1 and SLIM2 variants of MGU are more stable than those of GRU and LSTM. While, the SLIM3 variant of LSTM is more stable than the SLIM3 variant of MGU and GRU.

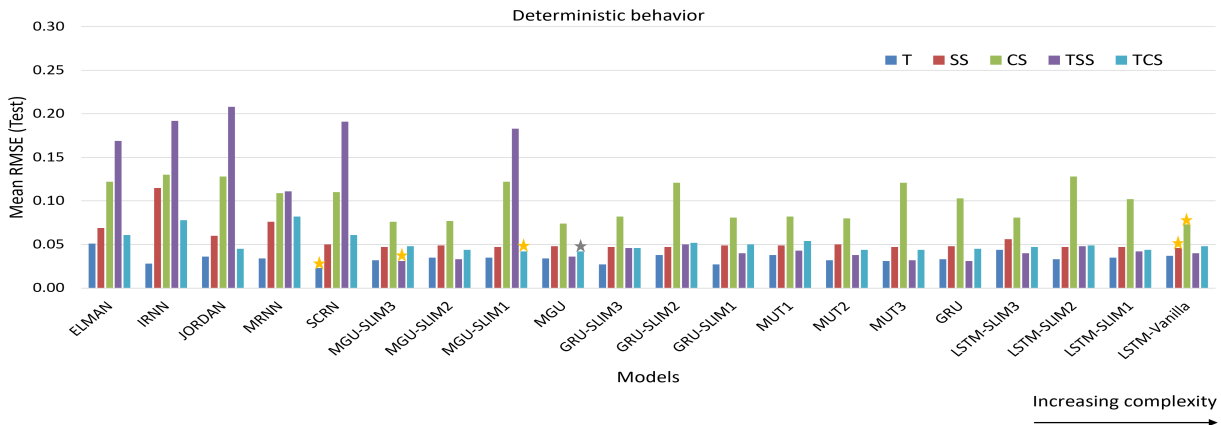


Figure 19: Forecasting performance of RNN cell structures with respect to time series with deterministic behavior generated by 5 types of DGPs: T, SS, CS, TSS, and TCS.

With regard to the nonlinear behavior, all the models express similar abilities in forecasting the 6 nonlinear time series patterns (Figure 21). Their forecasting errors decrease with the increase in the nonlinear order of the time series. However, the JORDAN and SCRNN models find some difficulties in learning the STAR process compared to the other models.

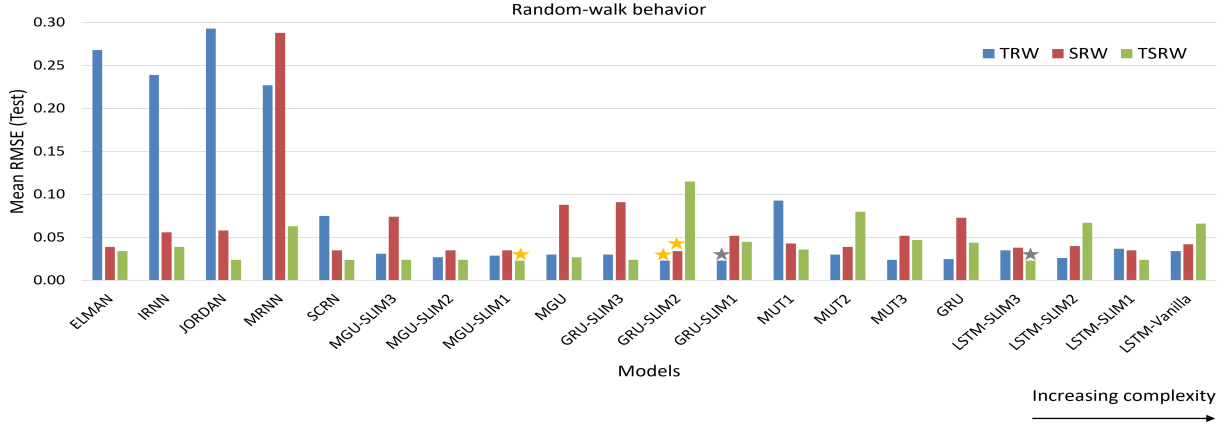


Figure 20: Forecasting performance of RNN cell structures with respect to time series with random-walk behavior generated by 3 types of DGPs: TRW, SRW, and TSRW.

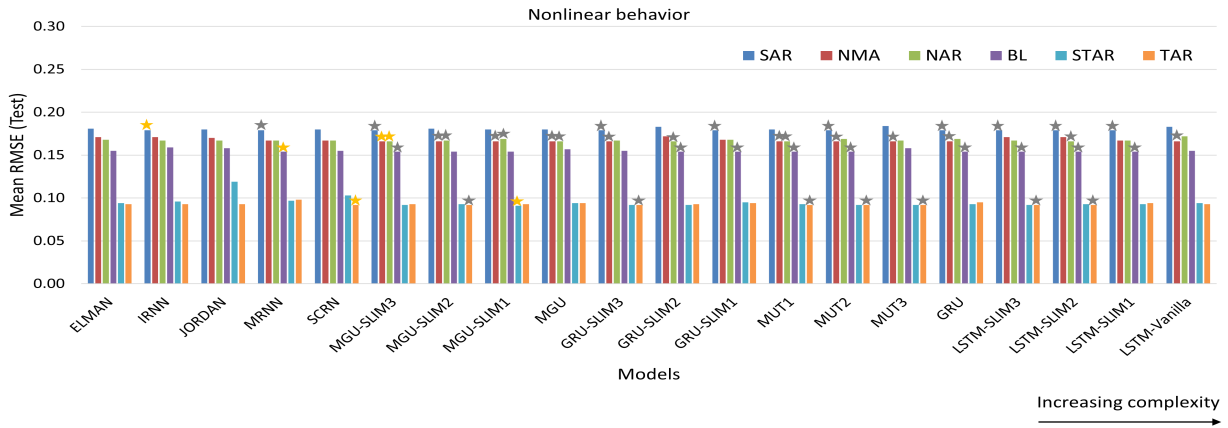


Figure 21: Forecasting performance of RNN cell structures with respect to time series with nonlinear behavior generated by 6 types of DGPs: SAR(2), NMA(2), NAR(2), BL(2), STAR(2), and TAR(2).

Similar findings can be noticed with the long-memory time series patterns where all the models express similar behavior (Figure 22). Their forecasting errors decrease with the increase in the long-range dependency order of the ARFIMA process. Although, the MRNN model shows an opposite behavior due to the occurrence of the vanishing gradient problem. Eventually, for the chaotic behavior, the RNN models exhibit approximately the same performance with regard to the 4 chaotic processes (Figure 23). In almost all RNN models, the Mackey-Glass process followed by the Hénon process are more challenging compared to the Rössler process followed by the Lorenz process. Nevertheless, the forecasting error of the Hénon process exceeds the one of the Mackey-Glass process with the following models: IRNN, MGU-SLIM1, GRU-SLIM3, GRU-SLIM1, and MUT2. In addition, the ELMAN, MRNN, and SCRNN models demonstrate poor performance in forecasting the Rössler process compared to the remaining models.

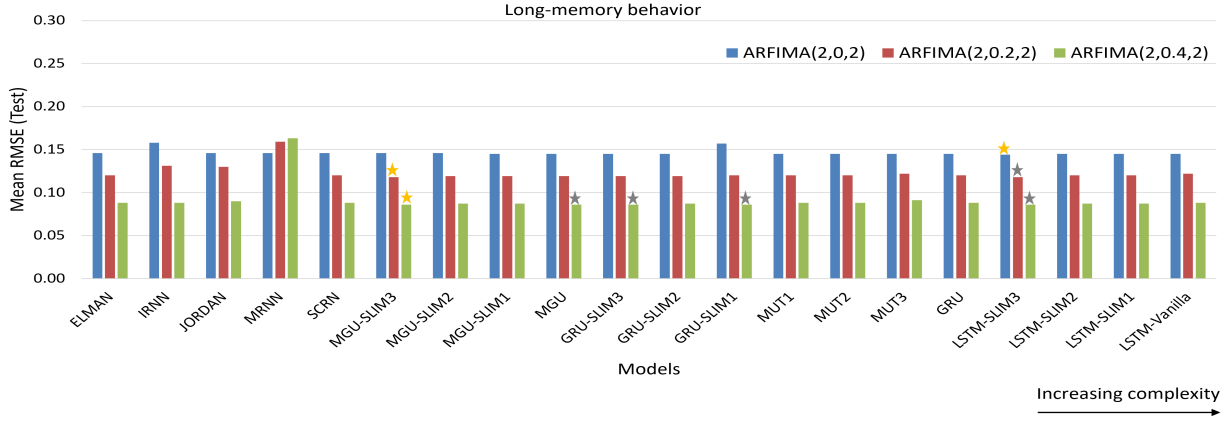


Figure 22: Forecasting performance of RNN cell structures with respect to time series with long-memory behavior generated by 3 types of DGPs using ARFIMA with $d = \{0, 0.2, 0.4\}$.

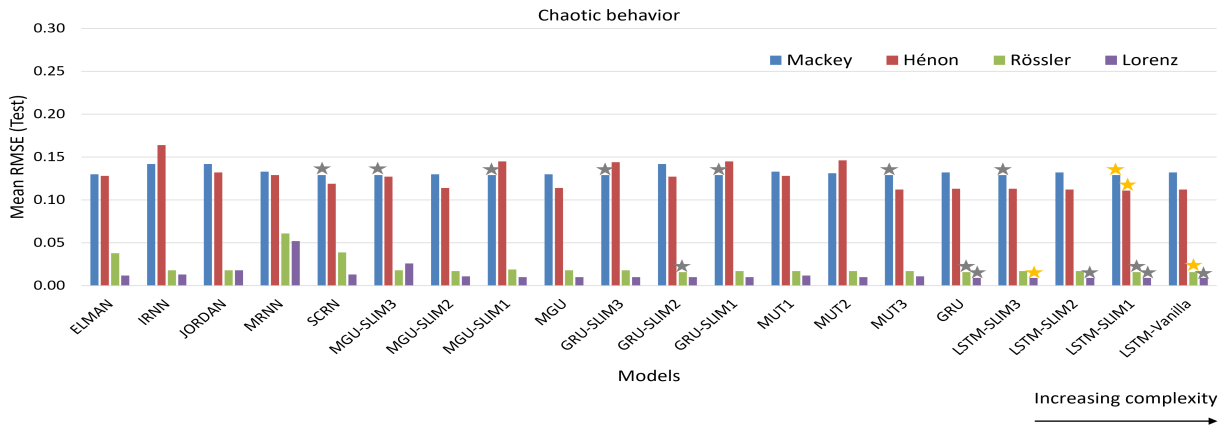


Figure 23: Forecasting performance of RNN cell structures with respect to time series with noisy chaotic behavior generated by 4 types of DGPs: Mackey-Glass , Lorenz, Rössler, and Hénon map.

To examine the general ability of RNN models with respect to each behavior, we present the overall mean RMSE over all the DGPs of each behavior in Figure 24. To model the deterministic behavior, MGU-SLIM3 is the most advocated, nevertheless, the simple RNN models (ELMAN, IRNN, JORDAN, MRNN, and SCRNN) and the MGU-SLIM1 model should be avoided. To predict the random-walk behavior, the MGU-SLIM2 model is the most recommended, and the following models should be avoided: ELMAN, IRNN, JORDAN, and MRNN. To capture the nonlinear behavior, all the RNN models present similar performance, while MGU-SLIM3 is the most performing. To forecast the long memory behavior, almost all the RNN models exhibit similar results, such that MRNN is the less performing. However, the most recommended model is LSTM-SLIM3. To model the Chaotic behavior in time series, LSTM-SLIM1 is the most suitable. In Table 13, we provide guidelines about the best RNN model to be used with each process and with each behavior.

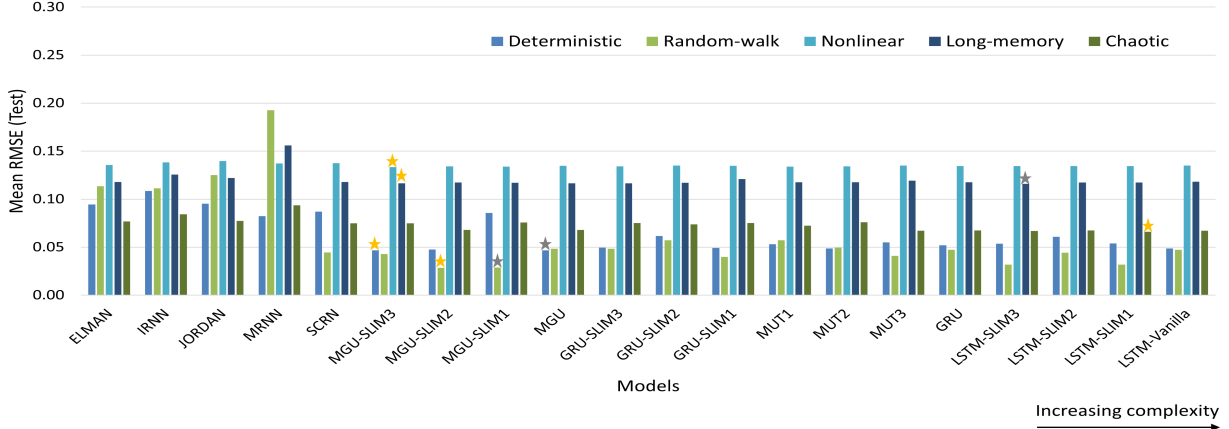


Figure 24: Average forecasting performance of RNN cell structures with respect to five time series behaviors.

The results of the two experiments are summarized in Table 14. Over all the DGPs of the deterministic and the nonlinear behaviors, the most recommended cell is the SLIM3 version of MGU cell. For time series with random-walk behavior, both CIFG and MGU-SLIM2 cells exhibited similar forecasting abilities, however, we suggest to use MGU-SLIM2 cell since it is simpler than CIFG. Eventually, FB1 and LSTM-SLIM1 are the most recommended for long-memory and chaotic behaviors, respectively.

Based on the outcomes of the two experiments, we can also derive insights about the predictability of each behavior. In Figure 25, we present the average forecasting errors over all the 31 RNN structures used in this study for each of the five time series behaviors. We can notice that all the behaviors have different degrees of predictability. The most straightforward is the random-walk followed by the deterministic behavior. Then, the chaotic behavior is ranked in the third place followed by the long-memory behavior. Finally, the most challenging one is the nonlinear behavior.

Table 14: Summary of the results of the two experiments.

Behaviors	Experiment 1		Experiment 2		Recommended cell
	Best cell	RMSE	Best cell	RMSE	
Deterministic	CIFG	0.048	MGU-SLIM3	0.0468	MGU-SLIM3
Random-walk	CIFG	0.0286	MGU-SLIM2	0.0286	MGU-SLIM2
Nonlinear	NOG	0.1418	MGU-SLIM3	0.1333	MGU-SLIM3
Long-memory	FB1	0.1163	MGU-SLIM3	0.1166	FB1
Chaotic	NOAF	0.0667	LSTM-SLIM1	0.0662	LSTM-SLIM1

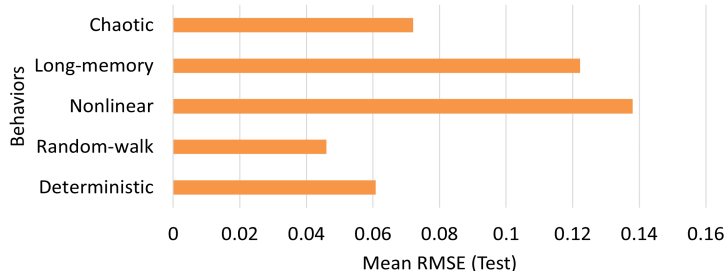


Figure 25: Average forecasting error over all the 31 RNN cells with respect to each time series behavior.

7. Conclusions

In this paper, we proposed a comprehensive taxonomy of all possible time series behaviors, which are: deterministic, random-walk, nonlinear, long-memory, and chaotic. Then, we conducted two experiments to show the best RNN cell structure for each behavior. In the first experiment, we evaluated LSTM-Vanilla model and 11 of its variants created based on one alteration in its basic architecture that consists in (1) removing (NIG, NFG, NOG, NIAF, NFAF, NOAF, and NCAF), (2) adding (PC and FGR), or (3) substituting (FB1 and CIFG) one cell component. While, in the second experiment, we evaluated LSTM-Vanilla along with a set of 19 RNN models based on other recurrent cell structures (JORDAN, ELMAN, MRNN, SCRNN, IRNN, GRU, MGU, MUT1, MUT2, MUT3, and 9 SLIM variants).

In the first experiment, We showed that CIFG cell is the most suitable for non-stationary time series due to the existence of deterministic behavior or random-walk behavior. We also, experimentally, proved that all the LSTM-Vanilla cells have approximately comparable forecasting ability in the case of nonlinear behavior, such that NOG is the most stable. The obtained results showed that the output activation function is a critical component that help LSTM cell capture long term dependencies. In the same context, we demonstrated that FB1 cell is the most recommended in forecasting time series with long-term behavior. Eventually, we demonstrated that to forecast time series with chaotic behavior, the output activation function should be removed since the NOAF cell displayed the best results.

In the second experiment, over the 20 evaluated RNN models, the best forecasting results were achieved by the new parameter-reduced variants of MGU and LSTM. With time series of deterministic, nonlinear, and long memory behaviors, the best cell was MGU-SLIM3. For the random-walk behavior, the most performing model was based on MGU-SLIM2 cell. Finally, for chaotic behavior, RNN model-based LSTM-SLIM1 cell outperformed all the other models.

Based on the outcomes of both experiments, we arrived to demonstrate that the SLIM3 version of MGU cell has the highest ability to increase the performance of RNN model in forecasting deterministic and nonlinear behaviors. While, its SLIM2 version is recommended in the case of time series with random-walk behavior. Finally, for the long-memory and the chaotic behaviors, FB1 and LSTM-SLIM1 cells are strongly advocated, respectively. The outcomes of our study are limited to the time series with a single behavior.

However, in real-world problems, combined behaviors (i.e., more than one behavior in the same time series) can also occur. As future work, evaluating the best RNN cell with respect to such types of time series can complement the guidelines provided by this study.

Acknowledgements

This work was partially supported by DETECTOR (A-RNM-256-UGR18 Universidad de Granada/FEDER), LifeWatch SmartEcomountains (LifeWatch-2019-10-UGR-01 Ministerio de Ciencia e Innovación/Universidad de Granada/FEDER), DeepL-ISCO (A-TIC-458-UGR18 Ministerio de Ciencia e Innovación/FEDER), BigDDL-CET (P18-FR-4961 Ministerio de Ciencia e Innovación/Universidad de Granada/FEDER).

References

- S. Abdulkarim. Time series prediction with simple recurrent neural networks. *Bayero Journal of Pure and Applied Sciences*, 9(1):19–24, 2016.
- G. Alkhatat and R. Mehmood. A review and taxonomy of wind and solar energy forecasting methods based on deep learning. *Energy and AI*, page 100060, 2021.
- S. Athiyarath, M. Paul, and S. Krishnaswamy. A comparative study and analysis of time series forecasting techniques. *SN Computer Science*, 1:1–7, 2020.
- A. Bensaïda and H. Litimi. High level chaos in the exchange and index markets. *Chaos, Solitons & Fractals*, 54:90–95, 2013.
- F. M. Bianchi, E. Maiorino, M. C. Kampffmeyer, A. Rizzi, and R. Jenssen. An overview and comparative analysis of recurrent neural networks for short term load forecasting. *arXiv preprint arXiv:1705.04378*, 2017.
- A. Blumer, A. Ehrenfeucht, D. Haussler, and M. K. Warmuth. Occam’s razor. *Information processing letters*, 24(6):377–380, 1987.
- B. Boaretto, R. C. Budzinski, K. L. Rossi, T. L. Prado, S. R. Lopes, and C. Masoller. Discriminating chaotic and stochastic time series using permutation entropy and artificial neural networks. *Scientific reports*, 11(1):1–10, 2021.
- M. Bourdeau, X. qiang Zhai, E. Nefzaoui, X. Guo, and P. Chatellier. Modeling and forecasting building energy consumption: A review of data-driven techniques. *Sustainable Cities and Society*, 48:101533, 2019.
- G. E. Box, G. M. Jenkins, G. C. Reinsel, and G. M. Ljung. *Time series analysis: forecasting and control*. John Wiley & Sons, 2015.

- A. H. Bukhari, M. A. Z. Raja, M. Sulaiman, S. Islam, M. Shoaib, and P. Kumam. Fractional neuro-sequential arfima-lstm for financial market forecasting. *IEEE Access*, 8:71326–71338, 2020.
- M. Cencini, M. Falcioni, E. Olbrich, H. Kantz, and A. Vulpiani. Chaos or noise: Difficulties of a distinction. *Physical Review E*, 62(1):427, 2000.
- R. Chandra and M. Zhang. Cooperative coevolution of elman recurrent neural networks for chaotic time series prediction. *Neurocomputing*, 86:116–123, 2012.
- C. Chatfield. *The analysis of time series: theory and practice*. Springer, 2013.
- V. K. R. Chimmula and L. Zhang. Time series forecasting of covid-19 transmission in canada using lstm networks. *Chaos, Solitons & Fractals*, 135:109864, 2020.
- K. Cho, B. Van Merriënboer, C. Gulcehre, D. Bahdanau, F. Bougares, H. Schwenk, and Y. Bengio. Learning phrase representations using rnn encoder-decoder for statistical machine translation. *arXiv preprint arXiv:1406.1078*, 2014.
- B. Choubin, G. Zehtabian, A. Azareh, E. Rafiei-Sardooi, F. Sajedi-Hosseini, and Ö. Kişi. Precipitation forecasting using classification and regression trees (cart) model: a comparative study of different approaches. *Environmental earth sciences*, 77(8):1–13, 2018.
- S. Crone. Nn5 forecasting competition for artificial neural networks & computational intelligence, 2008.
- H. A. Dau, A. Bagnall, K. Kamgar, C.-C. M. Yeh, Y. Zhu, S. Gharghabi, C. A. Ratanamahatana, and E. Keogh. The ucr time series archive. *IEEE/CAA Journal of Automatica Sinica*, 6(6):1293–1305, 2019.
- R. Dey and F. M. Salem. Gate-variants of gated recurrent unit (gru) neural networks. In *2017 IEEE 60th international midwest symposium on circuits and systems (MWSCAS)*, pages 1597–1600. IEEE, 2017.
- D. A. Dickey and W. A. Fuller. Distribution of the estimators for autoregressive time series with a unit root. *Journal of the American statistical association*, 74(366a):427–431, 1979.
- F. Divina, M. Garcia Torres, F. A. Gómez Vela, and J. L. Vazquez Noguera. A comparative study of time series forecasting methods for short term electric energy consumption prediction in smart buildings. *Energies*, 12(10):1934, 2019.
- G. Dudek. Neural networks for pattern-based short-term load forecasting: A comparative study. *Neurocomputing*, 205:64–74, 2016.
- J.-P. Eckmann and D. Ruelle. Ergodic theory of chaos and strange attractors. *The theory of chaotic attractors*, pages 273–312, 1985.

- J. L. Elman. Finding structure in time. *Cognitive science*, 14(2):179–211, 1990.
- M. Erdelj, M. Król, and E. Natalizio. Wireless sensor networks and multi-uav systems for natural disaster management. *Computer Networks*, 124:72–86, 2017.
- T. Fischer, C. Krauss, and A. Treichel. Machine learning for time series forecasting—a simulation study. Technical report, FAU Discussion Papers in Economics, 2018.
- F. A. Gers and E. Schmidhuber. Lstm recurrent networks learn simple context-free and context-sensitive languages. *IEEE Transactions on Neural Networks*, 12(6):1333–1340, 2001.
- F. A. Gers and J. Schmidhuber. Recurrent nets that time and count. In *Proceedings of the IEEE-INNS-ENNS International Joint Conference on Neural Networks. IJCNN 2000. Neural Computing: New Challenges and Perspectives for the New Millennium*, volume 3, pages 189–194. IEEE, 2000.
- F. A. Gers, J. Schmidhuber, and F. Cummins. Learning to forget: Continual prediction with lstm. *Neural computation*, 12(10):2451–2471, 2000.
- F. A. Gers, N. N. Schraudolph, and J. Schmidhuber. Learning precise timing with lstm recurrent networks. *Journal of machine learning research*, 3(Aug):115–143, 2002.
- J. Geweke and S. Porter-Hudak. The estimation and application of long memory time series models. *Journal of time series analysis*, 4(4):221–238, 1983.
- F. Giuliari, I. Hasan, M. Cristani, and F. Galasso. Transformer networks for trajectory forecasting. In *2020 25th International Conference on Pattern Recognition (ICPR)*, pages 10335–10342. IEEE, 2021.
- R. Godahewa, C. Bergmeir, and G. Webb. Cif 2016 dataset, June 2020. URL <https://doi.org/10.5281/zenodo.3904073>.
- R. Godahewa, C. Bergmeir, G. I. Webb, R. J. Hyndman, and P. Montero-Manso. Monash time series forecasting archive. *arXiv preprint arXiv:2105.06643*, 2021.
- G. A. Gottwald and I. Melbourne. A new test for chaos in deterministic systems. *Proceedings of the Royal Society of London. Series A: Mathematical, Physical and Engineering Sciences*, 460(2042):603–611, 2004.
- F. Granata. Evapotranspiration evaluation models based on machine learning algorithms—a comparative study. *Agricultural Water Management*, 217:303–315, 2019.
- P. Grassberger and I. Procaccia. Dimensions and entropies of strange attractors from a fluctuating dynamics approach. *Physica D: Nonlinear Phenomena*, 13(1-2):34–54, 1984.
- P. Grau-Carles. Tests of long memory: A bootstrap approach. *Computational Economics*, 25(1-2):103–113, 2005.

- A. Graves, G. Wayne, and I. Danihelka. Neural turing machines. *arXiv preprint arXiv:1410.5401*, 2014.
- K. Greff, R. K. Srivastava, J. Koutník, B. R. Steunebrink, and J. Schmidhuber. Lstm: A search space odyssey. *IEEE transactions on neural networks and learning systems*, 28(10):2222–2232, 2016.
- J. C. Heck and F. M. Salem. Simplified minimal gated unit variations for recurrent neural networks. In *2017 IEEE 60th International Midwest Symposium on Circuits and Systems (MWSCAS)*, pages 1593–1596. IEEE, 2017.
- S. Hochreiter and J. Schmidhuber. Long short-term memory. *Neural computation*, 9(8):1735–1780, 1997.
- L. Inglada-Perez. A comprehensive framework for uncovering non-linearity and chaos in financial markets: Empirical evidence for four major stock market indices. *Entropy*, 22(12):1435, 2020.
- K. Irie, Z. Tüske, T. Alkhouli, R. Schlüter, H. Ney, et al. Lstm, gru, highway and a bit of attention: an empirical overview for language modeling in speech recognition. In *Interspeech*, pages 3519–3523, 2016.
- L. Jing, C. Gulcehre, J. Peurifoy, Y. Shen, M. Tegmark, M. Soljagic, and Y. Bengio. Gated orthogonal recurrent units: On learning to forget. *Neural computation*, 31(4):765–783, 2019.
- M. Jordan. Serial order: A parallel distributed processing approach advances in connectionist theory, 1989.
- R. Jozefowicz, W. Zaremba, and I. Sutskever. An empirical exploration of recurrent network architectures. In *International conference on machine learning*, pages 2342–2350. PMLR, 2015.
- Y. Kang, R. J. Hyndman, and F. Li. Gratis: Generating time series with diverse and controllable characteristics. *Statistical Analysis and Data Mining: The ASA Data Science Journal*, 13(4):354–376, 2020.
- D. T. Kaplan. Exceptional events as evidence for determinism. *Physica D: Nonlinear Phenomena*, 73(1-2):38–48, 1994.
- D. M. Keenan. A tukey nonadditivity-type test for time series nonlinearity. *Biometrika*, 72(1):39–44, 1985.
- E. Keogh and S. Kasetty. On the need for time series data mining benchmarks: a survey and empirical demonstration. *Data Mining and knowledge discovery*, 7(4):349–371, 2003.
- R. Khaldi, A. El Afia, and R. Chiheb. Forecasting of btc volatility: comparative study between parametric and nonparametric models. *Progress in Artificial Intelligence*, 8(4):511–523, 2019a.
- R. Khaldi, A. El Afia, and R. Chiheb. Forecasting of weekly patient visits to emergency department: real case study. *Procedia computer science*, 148:532–541, 2019b.
- J.-M. Kim and H. Jung. Time series forecasting using functional partial least square regression with stochastic volatility, garch, and exponential smoothing. *Journal of Forecasting*, 37(3):269–280, 2018.

- D. Kwiatkowski, P. C. Phillips, P. Schmidt, and Y. Shin. Testing the null hypothesis of stationarity against the alternative of a unit root: How sure are we that economic time series have a unit root? *Journal of econometrics*, 54(1-3):159–178, 1992.
- Q. V. Le, N. Jaitly, and G. E. Hinton. A simple way to initialize recurrent networks of rectified linear units. *arXiv preprint arXiv:1504.00941*, 2015.
- Q. Li and R.-C. Lin. A new approach for chaotic time series prediction using recurrent neural network. *Mathematical Problems in Engineering*, 2016, 2016.
- T. P. Lim and S. Puthusserypady. Chaotic time series prediction and additive white gaussian noise. *Physics letters A*, 365(4):309–314, 2007.
- H. Liu, G. Yan, Z. Duan, and C. Chen. Intelligent modeling strategies for forecasting air quality time series: A review. *Applied Soft Computing*, page 106957, 2021.
- K. Liu, Y. Chen, and X. Zhang. An evaluation of arfima (autoregressive fractional integral moving average) programs. *Axioms*, 6(2):16, 2017.
- S. Liu, H. Ji, and M. C. Wang. Nonpooling convolutional neural network forecasting for seasonal time series with trends. *IEEE transactions on neural networks and learning systems*, 31(8):2879–2888, 2019.
- Y. Liu. Novel volatility forecasting using deep learning–long short term memory recurrent neural networks. *Expert Systems with Applications*, 132:99–109, 2019.
- A. W. Lo. Long-term memory in stock market prices. *Econometrica: Journal of the Econometric Society*, pages 1279–1313, 1991.
- C. López-Caraballo, I. Salfate, J. Lazzús, P. Rojas, M. Rivera, and L. Palma-Chilla. Mackey-glass noisy chaotic time series prediction by a swarm-optimized neural network. In *Journal of Physics: Conference Series*, volume 720, page 012002. IOP Publishing, 2016.
- Y. Lu and F. M. Salem. Simplified gating in long short-term memory (lstm) recurrent neural networks. In *2017 IEEE 60th International Midwest Symposium on Circuits and Systems (MWSCAS)*, pages 1601–1604. IEEE, 2017.
- Q.-L. Ma, Q.-L. Zheng, H. Peng, T.-W. Zhong, and L.-Q. Xu. Chaotic time series prediction based on evolving recurrent neural networks. In *2007 international conference on machine learning and cybernetics*, volume 6, pages 3496–3500. IEEE, 2007.
- K. Maeng, J. Kim, and J. Shin. Demand forecasting for the 5g service market considering consumer preference and purchase delay behavior. *Telematics and Informatics*, 47:101327, 2020.

- S. Makridakis, E. Spiliotis, and V. Assimakopoulos. The m4 competition: Results, findings, conclusion and way forward. *International Journal of Forecasting*, 34(4):802–808, 2018.
- B. B. Mandelbrot and J. R. Wallis. Noah, joseph, and operational hydrology. *Water resources research*, 4(5):909–918, 1968.
- M. Matilla-García and M. R. Marín. A new test for chaos and determinism based on symbolic dynamics. *Journal of Economic Behavior & Organization*, 76(3):600–614, 2010.
- T. Mikolov, A. Joulin, S. Chopra, M. Mathieu, and M. Ranzato. Learning longer memory in recurrent neural networks. *arXiv preprint arXiv:1412.7753*, 2014.
- D. C. Montgomery, C. L. Jennings, and M. Kulahci. *Introduction to time series analysis and forecasting*. John Wiley & Sons, 2015.
- M. Murat, I. Malinowska, M. Gos, and J. Krzyszczyk. Forecasting daily meteorological time series using arima and regression models. *International agrophysics*, 32(2), 2018.
- D. Neil, M. Pfeiffer, and S.-C. Liu. Phased lstm: Accelerating recurrent network training for long or event-based sequences. *arXiv preprint arXiv:1610.09513*, 2016.
- O. Nina and A. Rodriguez. Simplified lstm unit and search space probability exploration for image description. In *2015 10th International Conference on Information, Communications and Signal Processing (ICICSP)*, pages 1–5. IEEE, 2015.
- R. S. Olson, W. La Cava, P. Orzechowski, R. J. Urbanowicz, and J. H. Moore. Pmlb: a large benchmark suite for machine learning evaluation and comparison. *BioData mining*, 10(1):1–13, 2017.
- W. Palma. *Long-memory time series: theory and methods*, volume 662. John Wiley & Sons, 2007.
- G. Papacharalampous and H. Tyralis. Hydrological time series forecasting using simple combinations: Big data testing and investigations on one-year ahead river flow predictability. *Journal of Hydrology*, 590:125205, 2020.
- A. R. S. Parmezan, V. M. Souza, and G. E. Batista. Evaluation of statistical and machine learning models for time series prediction: Identifying the state-of-the-art and the best conditions for the use of each model. *Information sciences*, 484:302–337, 2019.
- R. Pascanu, T. Mikolov, and Y. Bengio. On the difficulty of training recurrent neural networks. In *International conference on machine learning*, pages 1310–1318. PMLR, 2013.
- C.-K. Peng, S. V. Buldyrev, S. Havlin, M. Simons, H. E. Stanley, and A. L. Goldberger. Mosaic organization of dna nucleotides. *Physical review e*, 49(2):1685, 1994.

- P. C. Phillips and P. Perron. Testing for a unit root in time series regression. *Biometrika*, 75(2):335–346, 1988.
- A. Pulver and S. Lyu. Lstm with working memory. In *2017 International Joint Conference on Neural Networks (IJCNN)*, pages 845–851. IEEE, 2017.
- Z. Qu. A test against spurious long memory. *Journal of Business & Economic Statistics*, 29(3):423–438, 2011.
- R. A. Rajagukguk, R. A. Ramadhan, and H.-J. Lee. A review on deep learning models for forecasting time series data of solar irradiance and photovoltaic power. *Energies*, 13(24):6623, 2020.
- N. Ramakrishnan and T. Soni. Network traffic prediction using recurrent neural networks. In *2018 17th IEEE International Conference on Machine Learning and Applications (ICMLA)*, pages 187–193. IEEE, 2018.
- J. Runge and R. Zmeureanu. A review of deep learning techniques for forecasting energy use in buildings. *Energies*, 14(3):608, 2021.
- A. Sagheer and M. Kotb. Time series forecasting of petroleum production using deep lstm recurrent networks. *Neurocomputing*, 323:203–213, 2019.
- R. Salles, K. Belloze, F. Porto, P. H. Gonzalez, and E. Ogasawara. Nonstationary time series transformation methods: An experimental review. *Knowledge-Based Systems*, 164:274–291, 2019.
- M. Sangiorgio, F. Dercole, and G. Guariso. Forecasting of noisy chaotic systems with deep neural networks. *Chaos, Solitons & Fractals*, 153:111570, 2021.
- O. B. Sezer, M. U. Gudelek, and A. M. Ozbayoglu. Financial time series forecasting with deep learning: A systematic literature review: 2005–2019. *Applied Soft Computing*, 90:106181, 2020.
- S. Siami-Namini and A. S. Namin. Forecasting economics and financial time series: Arima vs. lstm. *arXiv preprint arXiv:1803.06386*, 2018.
- E. Spiliotis, A. Kouloumos, V. Assimakopoulos, and S. Makridakis. Are forecasting competitions data representative of the reality? *International Journal of Forecasting*, 36(1):37–53, 2020.
- I. Sutskever, O. Vinyals, and Q. V. Le. Sequence to sequence learning with neural networks. In *Advances in neural information processing systems*, pages 3104–3112, 2014.
- T. Teräsvirta, C.-F. Lin, and C. W. Granger. Power of the neural network linearity test. *Journal of time series analysis*, 14(2):209–220, 1993.
- Z. Tian. Chaotic characteristic analysis of short-term wind speed time series with different time scales. *Energy Sources, Part A: Recovery, Utilization, and Environmental Effects*, pages 1–15, 2019.

- R. S. Tsay. Nonlinearity tests for time series. *Biometrika*, 73(2):461–466, 1986.
- V. Veeriah, N. Zhuang, and G.-J. Qi. Differential recurrent neural networks for action recognition. In *Proceedings of the IEEE international conference on computer vision*, pages 4041–4049, 2015.
- O. Vinyals, A. Toshev, S. Bengio, and D. Erhan. Show and tell: A neural image caption generator. In *Proceedings of the IEEE conference on computer vision and pattern recognition*, pages 3156–3164, 2015.
- D. J. Wales. Calculating the rate of loss of information from chaotic time series by forecasting. *Nature*, 350(6318):485–488, 1991.
- Y.-C. Wang and T.-C. T. Chen. A direct-solution fuzzy collaborative intelligence approach for yield forecasting in semiconductor manufacturing. *Procedia Manufacturing*, 17:110–117, 2018.
- Z. Wang, N. Fathollahzadeh Attar, K. Khalili, J. Behmanesh, S. S. Band, A. Mosavi, and K.-w. Chau. Monthly streamflow prediction using a hybrid stochastic-deterministic approach for parsimonious nonlinear time series modeling. *Engineering Applications of Computational Fluid Mechanics*, 14(1):1351–1372, 2020.
- P. J. Werbos. Backpropagation through time: what it does and how to do it. *Proceedings of the IEEE*, 78(10):1550–1560, 1990.
- J. Weston, S. Chopra, and A. Bordes. Memory networks. *arXiv preprint arXiv:1410.3916*, 2014.
- H. White. An additional hidden unit test for neglected nonlinearity in multilayer feedforward networks. In *Proceedings of the international joint conference on neural networks*, volume 2, pages 451–455. Washington, DC, 1989.
- P. T. Yamak, L. Yujian, and P. K. Gadosey. A comparison between arima, lstm, and gru for time series forecasting. In *Proceedings of the 2019 2nd International Conference on Algorithms, Computing and Artificial Intelligence*, pages 49–55, 2019.
- K. Yeo. Model-free prediction of noisy chaotic time series by deep learning. *arXiv preprint arXiv:1710.01693*, 2017.
- H. Yu, L. J. Ming, R. Sumei, and Z. Shuping. A hybrid model for financial time series forecasting—integration of ewt, arima with the improved abc optimized elm. *IEEE Access*, 8:84501–84518, 2020.
- G. P. Zhang and M. Qi. Neural network forecasting for seasonal and trend time series. *European journal of operational research*, 160(2):501–514, 2005.
- G. P. Zhang, B. E. Patuwo, and M. Y. Hu. A simulation study of artificial neural networks for nonlinear time-series forecasting. *Computers & Operations Research*, 28(4):381–396, 2001.

G.-B. Zhou, J. Wu, C.-L. Zhang, and Z.-H. Zhou. Minimal gated unit for recurrent neural networks. *International Journal of Automation and Computing*, 13(3):226–234, 2016.

L. Zunino, M. C. Soriano, and O. A. Rosso. Distinguishing chaotic and stochastic dynamics from time series by using a multiscale symbolic approach. *Physical Review E*, 86(4):046210, 2012.

Appendix A. Architectures of the studied RNN cells

In this section, we provide the cell structures of the different RNN models along with their cellular calculations. To understand the calculations, Table A.15 presents a depiction of the mathematical notations. To better understand the components inside LSTM-Vanilla cell, we present below the role of the main elements:

- Input state x_t : it contains the data features at time step t .
- Output state y_t : it contains the output of the model at time step t .
- Hidden state h_t : it represents the short term memory of the cell at time step t .
- Cell state c_t : it represents the long-term memory of the cell at time step t .
- Candidate cell state \tilde{c}_t : it contains the new information we can use to update the cell state at time step t .
- Input gate Γ_{i_t} : it filters from the current candidate cell state the information that should be used to update the current cell state.
- Forget gate Γ_{f_t} : it filters from the previous cell state the information that should be used to update the current cell state.
- Output gate Γ_{o_t} : it filters from the current cell state the information that should be exposed to the external network (the next time step and the next hidden and/or output layer).

Table A.15: Nomenclature

Symbol	Significance
x_t	the input state at time step t .
h_t	the hidden state at time step t .
y_t	the output state at time step t .
Γ_{i_t}	the input gate at time step t .
Γ_{f_t}	the forget gate at time step t .
Γ_{o_t}	the output gate at time step t .
Γ_{u_t}	the update gate at time step t .
Γ_{r_t}	the relevance gate at time step t .
c_t	the cell state at time step t .
\tilde{c}_t	the candidate cell state at time step t .
W_{xh}	the weight matrix between the input and the hidden states.
W_{hh}	the weight matrix between the previous and the current hidden states.

Table A.15: Nomenclature

Symbol	Significance
W_{hy}	the weight matrix between the hidden and the output states.
W_{yh}	the weight matrix between the output and the hidden states.
W_{xs}	the weight matrix between the input and the context states.
W_{sh}	the weight matrix between the context and the hidden states.
W_{sy}	the weight matrix between the context and the output states.
W_{xi}	the weight matrix between the input state and the input gate.
W_{hi}	the weight matrix between the hidden state and the input gate.
W_{xo}	the weight matrix between the input state and the output gate.
W_{ho}	the weight matrix between the hidden state and the output gate.
W_{xf}	the weight matrix between the input state and the forget gate.
W_{hf}	the weight matrix between the hidden state and the forget gate.
$W_{x\bar{c}}$	the weight matrix between the input state and the candidate cell state.
$W_{h\bar{c}}$	the weight matrix between the hidden state and the candidate cell state.
$W_{x\bar{h}}$	the weight matrix between the input state and the candidate hidden state.
$W_{h\bar{h}}$	the weight matrix between the hidden state and the candidate hidden state.
W_{ci}	the weight matrix between the cell state and the input gate.
W_{cf}	the weight matrix between the cell state and the forget gate.
W_{co}	the weight matrix between the cell state and the output gate.
W_{xu}	the weight matrix between the input state and the update gate.
W_{hu}	the weight matrix between the hidden state and the update gate.
W_{xr}	the weight matrix between the input state and the relevance gate.
W_{hr}	the weight matrix between the hidden state and the relevance gate.
W_{ii}	the weight matrix between the previous and the current input gates.
W_{ff}	the weight matrix between the previous and the current forget gates.
W_{oo}	the weight matrix between the previous and the current output gates.
W_{if}	the weight matrix between the previous input gate and the current forget gate.
W_{io}	the weight matrix between the previous input gate and the current output gate.
W_{fi}	the weight matrix between the previous forget gate and the current input gate.
W_{fo}	the weight matrix between the previous forget gate and the current output gate.
W_{oi}	the weight matrix between the previous output gate and the current input gate.
W_{of}	the weight matrix between the previous output gate and the current forget gate.
b_h	the bias related to the hidden state.
b_y	the bias related to the output state.
$b_{\bar{c}}$	the bias related to the candidate cell state.

Table A.15: Nomenclature

Symbol	Significance
$b_{\tilde{h}}$	the bias related to the candidate hidden state.
b_i	the bias related to the input gate.
b_o	the bias related to the output gate.
b_f	the bias related to the forget gate.
b_u	the bias related to the update gate.
b_r	the bias related to the relevance gate.
g	the activation function of the output state (the identity function).
\otimes	the point-wise multiplication (Hadamard product) presented in the figures as \odot .
σ	the sigmoid activation function.

Table A.16: Description of different LSTM-Vanilla cell structures created based on one change in its architecture.

Cell name	Cell architecture	Cell computations
LSTM-Vanilla		$\tilde{c}_t = \tanh(x_t \cdot W_{x\tilde{c}} + h_{t-1} \cdot W_{h\tilde{c}} + b_{\tilde{c}})$ $\Gamma_{i_t} = \sigma(x_t \cdot W_{xi} + h_{t-1} \cdot W_{hi} + b_i)$ $\Gamma_{f_t} = \sigma(x_t \cdot W_{xf} + h_{t-1} \cdot W_{hf} + b_f)$ $\Gamma_{o_t} = \sigma(x_t \cdot W_{xo} + h_{t-1} \cdot W_{ho} + b_o)$ $c_t = \Gamma_{f_t} \otimes c_{t-1} + \Gamma_{i_t} \otimes \tilde{c}_t$ $h_t = \Gamma_{o_t} \otimes \tanh(c_t)$
LSTM-NIG		$\tilde{c}_t = \tanh(x_t \cdot W_{x\tilde{c}} + h_{t-1} \cdot W_{h\tilde{c}} + b_{\tilde{c}})$ $\Gamma_{f_t} = \sigma(x_t \cdot W_{xf} + h_{t-1} \cdot W_{hf} + b_f)$ $\Gamma_{o_t} = \sigma(x_t \cdot W_{xo} + h_{t-1} \cdot W_{ho} + b_o)$ $c_t = \Gamma_{f_t} \otimes c_{t-1} + \tilde{c}_t$ $h_t = \Gamma_{o_t} \otimes \tanh(c_t)$
LSTM-NFG		$\tilde{c}_t = \tanh(x_t \cdot W_{x\tilde{c}} + h_{t-1} \cdot W_{h\tilde{c}} + b_{\tilde{c}})$ $\Gamma_{i_t} = \sigma(x_t \cdot W_{xi} + h_{t-1} \cdot W_{hi} + b_i)$ $\Gamma_{o_t} = \sigma(x_t \cdot W_{xo} + h_{t-1} \cdot W_{ho} + b_o)$ $c_t = c_{t-1} + \Gamma_{i_t} \otimes \tilde{c}_t$ $h_t = \Gamma_{o_t} \otimes \tanh(c_t)$

Table A.16: – Continued from previous page

Cell name	Cell architecture	Cell computations
LSTM-NOG		$\tilde{c}_t = \tanh(x_t \cdot W_{x\tilde{c}} + h_{t-1} \cdot W_{h\tilde{c}} + b_{\tilde{c}})$ $\Gamma_{i_t} = \sigma(x_t \cdot W_{x_i} + h_{t-1} \cdot W_{h_i} + b_i)$ $\Gamma_{f_t} = \sigma(x_t \cdot W_{x_f} + h_{t-1} \cdot W_{h_f} + b_f)$ $c_t = \Gamma_{f_t} \otimes c_{t-1} + \Gamma_{i_t} \otimes \tilde{c}_t$ $h_t = \tanh(c_t)$
LSTM-NIAF		$\tilde{c}_t = \tanh(x_t \cdot W_{x\tilde{c}} + h_{t-1} \cdot W_{h\tilde{c}} + b_{\tilde{c}})$ $\Gamma_{i_t} = \sigma(x_t \cdot W_{x_i} + h_{t-1} \cdot W_{h_i} + b_i)$ $\Gamma_{f_t} = \sigma(x_t \cdot W_{x_f} + h_{t-1} \cdot W_{h_f} + b_f)$ $\Gamma_{o_t} = \sigma(x_t \cdot W_{x_o} + h_{t-1} \cdot W_{h_o} + b_o)$ $c_t = \Gamma_{f_t} \otimes c_{t-1} + \Gamma_{i_t} \otimes \tilde{c}_t$ $h_t = \Gamma_{o_t} \otimes \tanh(c_t)$
LSTM-NFAF		$\tilde{c}_t = \tanh(x_t \cdot W_{x\tilde{c}} + h_{t-1} \cdot W_{h\tilde{c}} + b_{\tilde{c}})$ $\Gamma_{i_t} = \sigma(x_t \cdot W_{x_i} + h_{t-1} \cdot W_{h_i} + b_i)$ $\Gamma_{f_t} = \sigma(x_t \cdot W_{x_f} + h_{t-1} \cdot W_{h_f} + b_f)$ $\Gamma_{o_t} = \sigma(x_t \cdot W_{x_o} + h_{t-1} \cdot W_{h_o} + b_o)$ $c_t = \Gamma_{f_t} \otimes c_{t-1} + \Gamma_{i_t} \otimes \tilde{c}_t$ $h_t = \Gamma_{o_t} \otimes \tanh(c_t)$
LSTM-NOAF		$\tilde{c}_t = \tanh(x_t \cdot W_{x\tilde{c}} + h_{t-1} \cdot W_{h\tilde{c}} + b_{\tilde{c}})$ $\Gamma_{i_t} = \sigma(x_t \cdot W_{x_i} + h_{t-1} \cdot W_{h_i} + b_i)$ $\Gamma_{f_t} = \sigma(x_t \cdot W_{x_f} + h_{t-1} \cdot W_{h_f} + b_f)$ $\Gamma_{o_t} = \sigma(x_t \cdot W_{x_o} + h_{t-1} \cdot W_{h_o} + b_o)$ $c_t = \Gamma_{f_t} \otimes c_{t-1} + \Gamma_{i_t} \otimes \tilde{c}_t$ $h_t = \Gamma_{o_t} \otimes \tanh(c_t)$
LSTM-NCAF		$\tilde{c}_t = x_t \cdot W_{x\tilde{c}} + h_{t-1} \cdot W_{h\tilde{c}} + b_{\tilde{c}}$ $\Gamma_{i_t} = \sigma(x_t \cdot W_{x_i} + h_{t-1} \cdot W_{h_i} + b_i)$ $\Gamma_{f_t} = \sigma(x_t \cdot W_{x_f} + h_{t-1} \cdot W_{h_f} + b_f)$ $\Gamma_{o_t} = \sigma(x_t \cdot W_{x_o} + h_{t-1} \cdot W_{h_o} + b_o)$ $c_t = \Gamma_{f_t} \otimes c_{t-1} + \Gamma_{i_t} \otimes \tilde{c}_t$ $h_t = \Gamma_{o_t} \otimes \tanh(c_t)$

Table A.16: – Continued from previous page

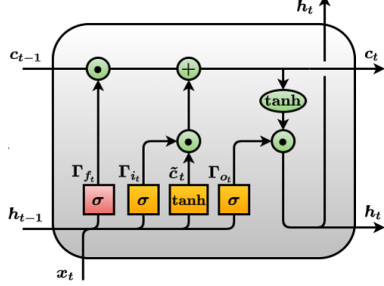
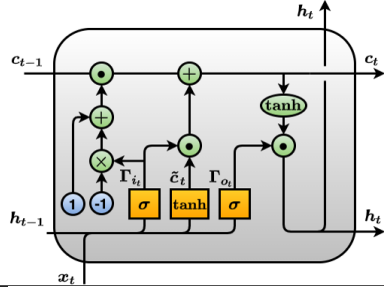
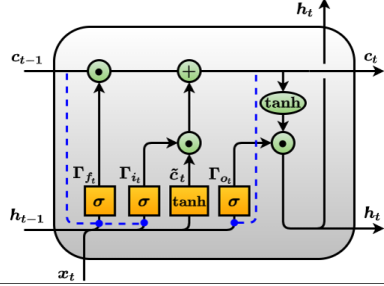
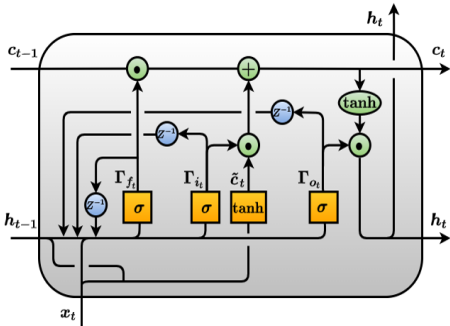
Cell name	Cell architecture	Cell computations
LSTM-FB1		$\tilde{c}_t = \tanh(x_t.W_{x\tilde{c}} + h_{t-1}.W_{h\tilde{c}} + b_{\tilde{c}})$ $\Gamma_{i_t} = \sigma(x_t.W_{xi} + h_{t-1}.W_{hi} + b_i)$ $b_f = 1$ $\Gamma_{f_t} = \sigma(x_t.W_{xf} + h_{t-1}.W_{hf} + b_f)$ $\Gamma_{o_t} = \sigma(x_t.W_{xo} + h_{t-1}.W_{ho} + b_o)$ $c_t = \Gamma_{f_t} \otimes c_{t-1} + \Gamma_{i_t} \otimes \tilde{c}_t$ $h_t = \Gamma_{o_t} \otimes \tanh(c_t)$
LSTM-CIFG		$\tilde{c}_t = \tanh(x_t.W_{x\tilde{c}} + h_{t-1}.W_{h\tilde{c}} + b_{\tilde{c}})$ $\Gamma_{i_t} = \sigma(x_t.W_{xi} + h_{t-1}.W_{hi} + b_i)$ $\Gamma_{o_t} = \sigma(x_t.W_{xo} + h_{t-1}.W_{ho} + b_o)$ $c_t = (1 - \Gamma_{i_t}) \otimes c_{t-1} + \Gamma_{i_t} \otimes \tilde{c}_t$ $h_t = \Gamma_{o_t} \otimes \tanh(c_t)$
LSTM-PC		$\tilde{c}_t = \tanh(x_t.W_{x\tilde{c}} + h_{t-1}.W_{h\tilde{c}} + b_{\tilde{c}})$ $\Gamma_{i_t} = \sigma(x_t.W_{xi} + h_{t-1}.W_{hi} + c_{t-1}.W_{ci} + b_i)$ $\Gamma_{f_t} = \sigma(x_t.W_{xf} + h_{t-1}.W_{hf} + c_{t-1}.W_{cf} + b_f)$ $\Gamma_{o_t} = \sigma(x_t.W_{xo} + h_{t-1}.W_{ho} + c_t.W_{co} + b_o)$ $c_t = \Gamma_{f_t} \otimes c_{t-1} + \Gamma_{i_t} \otimes \tilde{c}_t$ $h_t = \Gamma_{o_t} \otimes \tanh(c_t)$
LSTM-FGR		$\tilde{c}_t = \tanh(x_t.W_{x\tilde{c}} + h_{t-1}.W_{h\tilde{c}} + b_{\tilde{c}})$ $\Gamma_{i_t} = \sigma(x_t.W_{xi} + h_{t-1}.W_{hi} + \Gamma_{i_{(t-1)}}.W_{ii}$ $+ \Gamma_{f_{(t-1)}}.W_{fi} + \Gamma_{o_{(t-1)}}.W_{oi} + b_i)$ $\Gamma_{f_t} = \sigma(x_t.W_{xf} + h_{t-1}.W_{hf} + \Gamma_{i_{(t-1)}}.W_{if}$ $+ \Gamma_{f_{(t-1)}}.W_{ff} + \Gamma_{o_{(t-1)}}.W_{of} + b_f)$ $\Gamma_{o_t} = \sigma(x_t.W_{xo} + h_{t-1}.W_{ho} + \Gamma_{i_{(t-1)}}.W_{io}$ $+ \Gamma_{f_{(t-1)}}.W_{fo} + \Gamma_{o_{(t-1)}}.W_{oo} + b_o)$ $c_t = \Gamma_{f_t} \otimes c_{t-1} + \Gamma_{i_t} \otimes \tilde{c}_t$ $h_t = \Gamma_{o_t} \otimes \tanh(c_t)$

Table A.17: Description of different architectures of RNN cells.

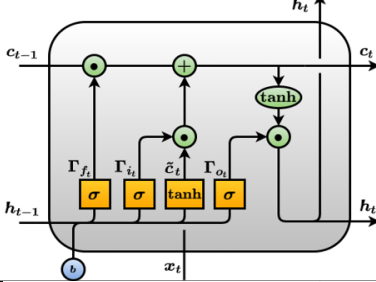
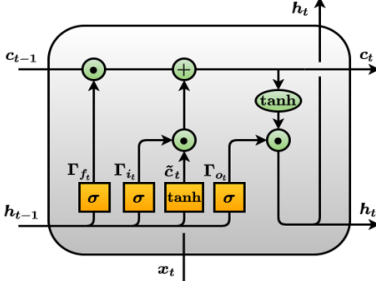
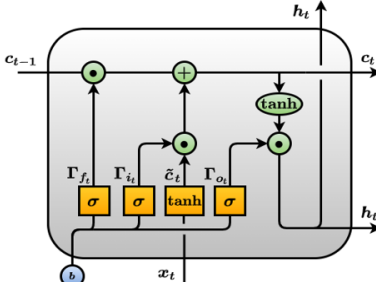
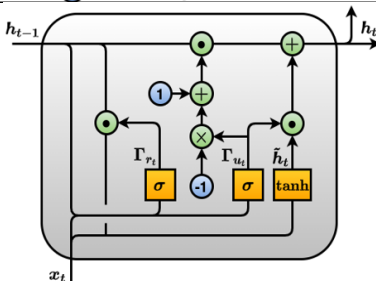
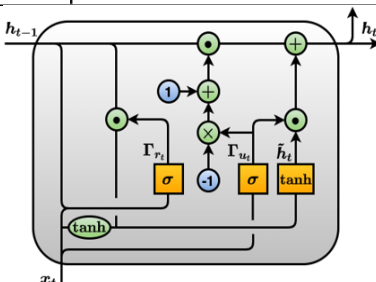
Cell name	Cell architecture	Cell computations
LSTM-SLIM1		$\tilde{c}_t = \tanh(x_t.W_{xc} + h_{t-1}.W_{hc} + b_{\tilde{c}})$ $\Gamma_{i_t} = \sigma(h_{t-1}.W_{hi} + b_i)$ $\Gamma_{f_t} = \sigma(h_{t-1}.W_{hf} + b_f)$ $\Gamma_{o_t} = \sigma(h_{t-1}.W_{ho} + b_o)$ $c_t = \Gamma_{f_t} \otimes c_{t-1} + \Gamma_{i_t} \otimes \tilde{c}_t$ $h_t = \Gamma_{o_t} \otimes \tanh(c_t)$
LSTM-SLIM2		$\tilde{c}_t = \tanh(x_t.W_{xc} + h_{t-1}.W_{hc} + b_{\tilde{c}})$ $\Gamma_{i_t} = \sigma(h_{t-1}.W_{hi})$ $\Gamma_{f_t} = \sigma(h_{t-1}.W_{hf})$ $\Gamma_{o_t} = \sigma(h_{t-1}.W_{ho})$ $c_t = \Gamma_{f_t} \otimes c_{t-1} + \Gamma_{i_t} \otimes \tilde{c}_t$ $h_t = \Gamma_{o_t} \otimes \tanh(c_t)$
LSTM-SLIM3		$\tilde{c}_t = \tanh(x_t.W_{xc} + h_{t-1}.W_{hc} + b_{\tilde{c}})$ $\Gamma_{i_t} = \sigma(b_i)$ $\Gamma_{f_t} = \sigma(b_f)$ $\Gamma_{o_t} = \sigma(b_o)$ $c_t = \Gamma_{f_t} \otimes c_{t-1} + \Gamma_{i_t} \otimes \tilde{c}_t$ $h_t = \Gamma_{o_t} \otimes \tanh(c_t)$
GRU		$\Gamma_{u_t} = \sigma(x_t.W_{xu} + h_{t-1}.W_{hu} + b_u)$ $\Gamma_{r_t} = \sigma(x_t.W_{xr} + h_{t-1}.W_{hr} + b_r)$ $\tilde{h}_t = \tanh(x_t.W_{x\tilde{h}} + (\Gamma_{r_t} \otimes h_{t-1}).W_{h\tilde{h}} + b_{\tilde{h}})$ $h_t = \Gamma_{u_t} \otimes \tilde{h}_t + (1 - \Gamma_{u_t}) \otimes h_{t-1}$
MUT1		$\Gamma_{u_t} = \sigma(x_t.W_{xu} + b_u)$ $\Gamma_{r_t} = \sigma(x_t.W_{xr} + h_{t-1}.W_{hr} + b_r)$ $\tilde{h}_t = \tanh(\tanh(x_t) + (\Gamma_{r_t} \otimes h_{t-1}).W_{h\tilde{h}} + b_{\tilde{h}})$ $h_t = \Gamma_{u_t} \otimes \tilde{h}_t + (1 - \Gamma_{u_t}) \otimes h_{t-1}$

Table A.17: – Continued from previous page

Cell name	Cell architecture	Cell computations
MUT2		$\Gamma_{u_t} = \sigma(x_t \cdot W_{xu} + h_{t-1} \cdot W_{hu} + b_u)$ $\Gamma_{r_t} = \sigma(x_t + h_{t-1} \cdot W_{hr} + b_r)$ $\tilde{h}_t = \tanh(x_t \cdot W_{x\tilde{h}} + (\Gamma_{r_t} \otimes h_{t-1}) \cdot W_{h\tilde{h}} + b_{\tilde{h}})$ $h_t = \Gamma_{u_t} \otimes \tilde{h}_t + (1 - \Gamma_{u_t}) \otimes h_{t-1}$
MUT3		$\Gamma_{u_t} = \sigma(x_t \cdot W_{xu} + \tanh(h_{t-1}) \cdot W_{hu} + b_u)$ $\Gamma_{r_t} = \sigma(x_t \cdot W_{xr} + h_{t-1} \cdot W_{hr} + b_r)$ $\tilde{h}_t = \tanh(x_t \cdot W_{x\tilde{h}} + (\Gamma_{r_t} \otimes h_{t-1}) \cdot W_{h\tilde{h}} + b_{\tilde{h}})$ $h_t = \Gamma_{u_t} \otimes \tilde{h}_t + (1 - \Gamma_{u_t}) \otimes h_{t-1}$
GRU-SLIM1		$\Gamma_{u_t} = \sigma(h_{t-1} \cdot W_{hu} + b_u)$ $\Gamma_{r_t} = \sigma(h_{t-1} \cdot W_{hr} + b_r)$ $\tilde{h}_t = \tanh(x_t \cdot W_{x\tilde{h}} + (\Gamma_{r_t} \otimes h_{t-1}) \cdot W_{h\tilde{h}} + b_{\tilde{h}})$ $h_t = \Gamma_{u_t} \otimes \tilde{h}_t + (1 - \Gamma_{u_t}) \otimes h_{t-1}$
GRU-SLIM2		$\Gamma_{u_t} = \sigma(h_{t-1} \cdot W_{hu})$ $\Gamma_{r_t} = \sigma(h_{t-1} \cdot W_{hr})$ $\tilde{h}_t = \tanh(x_t \cdot W_{x\tilde{h}} + (\Gamma_{r_t} \otimes h_{t-1}) \cdot W_{h\tilde{h}} + b_{\tilde{h}})$ $h_t = \Gamma_{u_t} \otimes \tilde{h}_t + (1 - \Gamma_{u_t}) \otimes h_{t-1}$
GRU-SLIM3		$\Gamma_{u_t} = \sigma(b_u)$ $\Gamma_{r_t} = \sigma(b_r)$ $\tilde{h}_t = \tanh(x_t \cdot W_{x\tilde{h}} + (\Gamma_{r_t} \otimes h_{t-1}) \cdot W_{h\tilde{h}} + b_{\tilde{h}})$ $h_t = \Gamma_{u_t} \otimes \tilde{h}_t + (1 - \Gamma_{u_t}) \otimes h_{t-1}$

Table A.17: – Continued from previous page

Cell name	Cell architecture	Cell computations
MGU		$\Gamma_{f_t} = \sigma(x_t \cdot W_{xf} + h_{t-1} \cdot W_{hf} + b_f)$ $\tilde{h}_t = \tanh(x_t \cdot W_{x\tilde{h}} + (\Gamma_{f_t} \otimes h_{t-1}) \cdot W_{h\tilde{h}} + b_{\tilde{h}})$ $h_t = \Gamma_{f_t} \otimes \tilde{h}_t + (1 - \Gamma_{f_t}) \otimes h_{t-1}$
MGU-SLIM1		$\Gamma_{f_t} = \sigma(h_{t-1} \cdot W_{hf} + b_f)$ $\tilde{h}_t = \tanh(x_t \cdot W_{x\tilde{h}} + (\Gamma_{f_t} \otimes h_{t-1}) \cdot W_{h\tilde{h}} + b_{\tilde{h}})$ $h_t = \Gamma_{f_t} \otimes \tilde{h}_t + (1 - \Gamma_{f_t}) \otimes h_{t-1}$
MGU-SLIM2		$\Gamma_{f_t} = \sigma(h_{t-1} \cdot W_{hf})$ $\tilde{h}_t = \tanh(x_t \cdot W_{x\tilde{h}} + (\Gamma_{f_t} \otimes h_{t-1}) \cdot W_{h\tilde{h}} + b_{\tilde{h}})$ $h_t = \Gamma_{f_t} \otimes \tilde{h}_t + (1 - \Gamma_{f_t}) \otimes h_{t-1}$
MGU-SLIM3		$\Gamma_{f_t} = \sigma(b_f)$ $\tilde{h}_t = \tanh(x_t \cdot W_{x\tilde{h}} + (\Gamma_{f_t} \otimes h_{t-1}) \cdot W_{h\tilde{h}} + b_{\tilde{h}})$ $h_t = \Gamma_{f_t} \otimes \tilde{h}_t + (1 - \Gamma_{f_t}) \otimes h_{t-1}$
SCRN		$s_t = (1 - \alpha)x_t \cdot W_{xs} + \alpha \cdot s_{t-1}$ $\alpha \in [0, 1]$ $h_t = \tanh(x_t \cdot W_{xh} + h_{t-1} \cdot W_{hh} + s_{t-1} \cdot W_{sh} + b_h)$

Table A.17: – Continued from previous page

Cell name	Cell architecture	Cell computations
MRNN		$h_t = \tanh(x_t \cdot W_{xh} + h_{t-1} \cdot W_{hh} + \hat{y}_{t-1} \cdot W_{yh} + b_h)$
JORDAN		$h_t = \tanh(x_t \cdot W_{xh} + \hat{y}_{t-1} \cdot W_{yh} + b_h)$
IRNN		$h_t = ReLu(x_t \cdot W_{xh} + h_{t-1} \cdot W_{hh} + b_h)$
ELMAN		$h_t = \tanh(x_t \cdot W_{xh} + h_{t-1} \cdot W_{hh} + b_h)$